Profiling withanolide A for therapeutic targets in neurodegenerative diseases

Crane, Erika A ; Heydenreuter, Wolfgang ; Beck, Katharina R ; Strajhar, Petra ; Vomacka, Jan ; Smiesko, Martin ; Mons, Elma ; Barth, Lydia ; Neuburger, Markus ; Vedani, Angelo ; Odermatt, Alex ; Sieber, Stephan A ; Gademann, Karl

Abstract: To identify new potential therapeutic targets for neurodegenerative diseases, we initiated activity-based protein profiling studies with withanolide A (WitA), a known neuritogenic constituent of Withania somnifera root with unknown mechanism of action. Molecular probes were designed and synthesized, and led to the discovery of the glucocorticoid receptor (GR) as potential target. Molecular modeling calculations using the VirtualToxLab predicted a weak binding affinity of WitA for GR. Neurite outgrowth experiments in human neuroblastoma SH-SY5Y cells further supported a glucocorticoid-dependent mechanism, finding that WitA was able to reverse the outgrowth inhibition mediated by dexamethasone (Dex). However, further GR binding and transactivation assays found no direct interference of WitA. Further molecular modeling analysis suggested that WitA, although forming several contacts with residues in the GR binding pocket, is lacking key stabilizing interactions as observed for Dex. Taken together, the data suggest that WitA-dependent induction of neurite outgrowth is not through a direct effect on GR, but might be mediated through a closely related pathway. Further experiments should evaluate a possible role of GR modulators and/or related signaling pathways such as ERK, Akt, NF- B, TR , or Hsp90 as potential targets in the WitA-mediated neuromodulatory effects.

DOI: https://doi.org/10.1016/j.bmc.2019.03.022

Profiling Withanolide A for Therapeutic Targets in Neurodegenerative Diseases

Erika A. Crane,[†] Wolfgang Heydenreuter,[ǂ] Katharina R. Beck,[‡] Petra Strajhar,[‡] Jan Vomacka,[ǂ] Martin Smiesko,[‡] Elma Mons,[†] Lydia Barth,[†] Markus Neuburger,[†] Angelo Vedani,[‡,⊥] Alex Odermatt,[‡] Stephan A. Sieber,[ǂ] and Karl Gademann*[§]

[†]Department of Chemistry, University of Basel, St. Johanns-Ring 19, CH-4056 Basel, Switzerland

[ǂ]Department of Chemistry, Centre for Integrated Protein Science (CIPSM), Institute for Advanced Studies (IAS), Technical University Munich, Lichtenbergstrasse 4, D-85747 Garching, Germany

[‡] Department of Pharmaceutical Sciences, University of Basel, Klingelbergstrasse 50, CH-4056 Basel, Switzerland

[⊥] Deceased June 28, 2016

[§]Department of Chemistry, University of Zurich, Winterthurerstrasse 190, CH-8057 Zürich, Switzerland

KEYWORDS withanolide A, target profiling, glucocorticoid receptor, neurotrophic agents

ABSTRACT: To identify new potential therapeutic targets for neurodegenerative diseases, we initiated activity-based protein profiling studies with withanolide A (WitA), a known neuritogenic constituent of *Withania somnifera* root with unknown mechanism of action. Molecular probes were designed and synthesized, and led to the discovery of the glucocorticoid receptor (GR) as potential target. Molecular modeling calculations using the *VirtualToxLab* predicted a weak binding affinity of WitA for GR. Neurite outgrowth experiments in human neuroblastoma SH-SY5Y cells further supported a glucocorticoid-dependent mechanism, finding that WitA was able to reverse the outgrowth inhibition mediated by dexamethasone (Dex). However, further GR binding and transactivation assays found no direct interference of WitA. Further molecular modeling analysis suggested that WitA, although forming several contacts with residues in the GR binding pocket, is lacking key stabilizing interactions as observed for Dex. Taken together, the data suggest that WitA-dependent induction of neurite outgrowth is not through a direct effect on GR, but might be mediated through a closely related pathway. Further experiments should evaluate a possible role of GR modulators and/or related signaling pathways such as ERK, Akt, NF-κB, TRα, or Hsp90 as potential targets in the WitA-mediated neuromodulatory effects.

1. Introduction

There has been a worldwide escalation over the past century in the prevalence of neurodegenerative diseases, such as Alzheimer's, Parkinson's and Huntington's disease.[1-4] However, there are still no cures for these disorders and current treatment options are only palliative. So far, drug discovery efforts have focused on small molecules that mimic neurotrophic properties of established polypeptidal therapeutics, as they possess inherently better pharmacological properties, mainly the ability to cross the blood-brain barrier.[1,5-10] More specifically, natural products or fragments thereof have become of special interest.[11-18] Thus, we became interested in withanolide A (WitA, **1**, Figure 1), one of the most bioactive constituents in *Withania somnifera*, also known as Ashwagandha root, Indian ginseng or winter cherry.[19-22] This ayurvedic herb has been used for centuries to treat a variety of ailments from arthritis, anxiety, insomnia, tuberculosis, asthma, to fibromyalgia, among others.[21,23,24] Even today, it is sold at yogi or organic shops in the form of herbal supplements or in teas as anti-inflammatory treatment, for cognition improvement and anti-aging effects, increase in sexual desire and fertility, among others.[21,25,26] A major steroidal component of this root, WitA, was isolated in 1971 from the roots of *Withania somnifera* (L.) DUNAL.[19] This compound is one of the 900 naturally occurring withanolides, a family of C_{28} steroids characterized by an ergostane skeleton and common functionalization at C1, C22 and C26.[27,28] Approximately 550 of these withanolides are considered "classic" or "unmodified", with a four-ringed steroidal core (ABCD) and an appended δ-lactone ring (E). They are known for their antitumor, anti-inflammatory, neuroprotective, immunomodulatory and insect anti-feedent activities, due to well-documented antiproliferative, neurite-outgrowth, and cholinesterase inhibitory activities.[23,25,27,29-33] In particular, WitA possesses strong neuropharmacological properties, promoting neurite outgrowth, reversing neuritic atrophy and aiding in synapse reconstruction.[26,34,35] Furthermore, WitA has been suggested to modulate several targets involved in Alzheimer's disease such as downregulation of BACE1, upregulation of ADAM10 in primary rat cortical neurons, and the activity of several secretases.[36] Some of us completed a synthesis of WitA and performed synthetic studies to access derivatives, which were then evaluated for their neurite outgrowth potential.[37,38] However, our interest in this natural product extended to a desire to understand its underlying mechanism of action and elucidate further biological targets for broader applications, which we hoped to achieve through target identification of this natural product via affinity-based protein profiling (ABPP).[39-42]

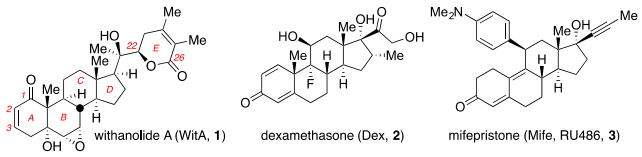

Figure 1. Structures of withanolide A (WitA, **1**), dexamethasone (Dex, **2**), and mifepristone (Mife, RU-486, **3**).

2. Results and discussion

2.1. Design of withanolide A molecular probes

WitA exhibits putative electrophilic moieties such as an epoxide and two Michael acceptor systems which could mediate target binding via covalent addition to corresponding nucleophilic amino acid residues in protein active sites. Therefore, the WitA core scaffold was functionalized with an alkyne handle at different positions and these probes were applied in gel-based and gel-free ABPP.[39-42] In this procedure, either SH-SY5Y human neuroblastoma or A549 human lung carcinoma cells were incubated for 1 to 20 hours with the probes at concentrations of 1–100 μM to enable labeling. The proteomes were then harvested and were bioorthogonally ligated to either a rhodamine- or biotin azide reporter tag through a Cu(I)-catalyzed [3+2] cycloaddition, or click chemistry, for visualization on fluorescent SDS-gels or mass-spectrometry (MS) based target identification, respectively.[43-45]

For a successful target profiling, the investigated compound needs to have a balanced reactivity and be modifiable with a sterically inert alkyne, distal from its reacting center.[41] The wide-ranging biological activities of the withanolides have been strongly linked to covalent modification and thorough analysis of structure-activity relationship (SAR) data revealed that the 2-ene-1-one of the A-ring was essential for activity.[27] Due to several possible conjugate acceptors existing in the molecule and for completeness sake, both A- and E-ring probes were targeted. Our prior SAR investigations of WitA revealed that neurite outgrowth activity could be retained with simple C1-oximes, making these favorable targets for the A-ring probe synthesis.[38] These synthetic studies also revealed A-ring modification to be fairly facile, but functionalizing the C1 position was rather challenging. The δ-lactone was also found to be particularly stable, rendering its functionalization difficult. Ideally, the R group of the C1 oxime would be designed to lack bulk, otherwise risk disrupting possible binding interactions with the target(s) in the assay. In addition, the oxygenation pattern in the B ring could not be removed or modified to prevent important contacts in the binding pockets of the target(s) from being lost. The synthesis of inert probes was targeted as well for elucidation of potential off-target effects, by removing the conjugate acceptor ability of the molecule.

Scheme 1. Synthesis of WitA Molecular Probes for Target Profiling.

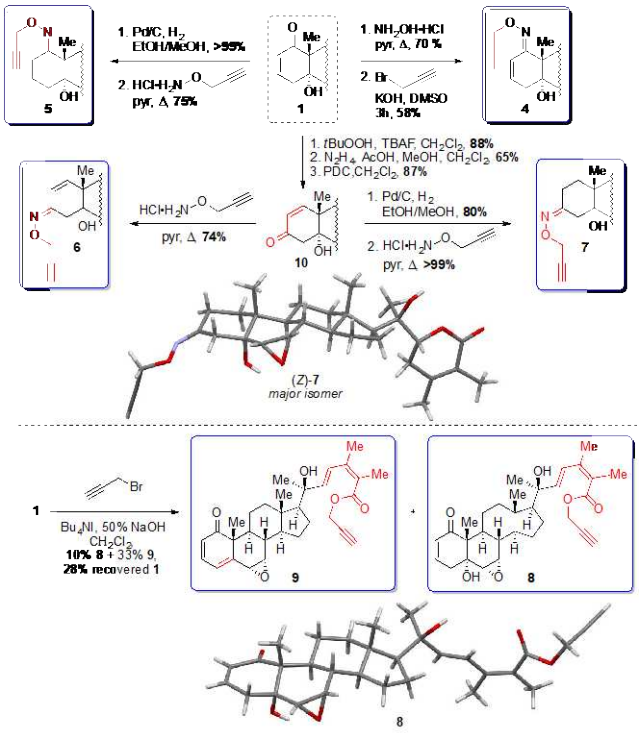

2.2 Synthesis of withanolide A molecular probes

For these synthetic studies, fresh WitA was isolated from powdered Ashwagandha root (0.038% yield, w/w) according to our previously published procedure.[37,38] In the synthesis of the A-ring probes, the unsaturated C1 propargyl oxime **4** was prepared in a two-step procedure with initial formation of the N-H oxime and then alkylation with propargyl bromide (Scheme 1). Direct formation of probe **4** was not possible, complimentary to what was observed in previous synthetic studies.[38] The corresponding saturated probe **5** was synthesized directly through propargyl oxime formation in a 75% yield, following a quantitative hydrogenation of WitA (**1**). The C3 probes were accessed through a Wharton transposition of WitA (**1**) and oxidation to form C3 enone **10**.[38] The unsaturated C3 propargyl oxime probe **6** could then be prepared directly in one step in a 74% yield. A mixture of oxime isomers was observed in this reaction after several hours, but the *E*-isomer could be exclusively obtained when the reaction time was extended (ca. 3 days). Similarly, saturated probe **7** was accessed in quantitative yield, following hydrogenation. We obtained a 3:2 ratio of separable *Z*:*E* oxime isomers. X-ray crystallography of the (*Z*)-**7** isomer confirmed the configuration assignment for each compound.[46] Only the *Z*-isomer of **7** was used in the target profiling and biological studies.

The E-ring probes were isolated from the same reaction in an attempt to alkylate the C20 tertiary alcohol under phase-transfer conditions. Propargyl ester **8** was formed during ring opening of the δ-lactone, while unsaturated propargyl ester **9**

was created through further elimination of the C5 hydroxyl group. The structure of ester **8** was confirmed by X-ray crystallography.[46]

2.3 Affinity-based protein profiling tests

The six molecular probes were then screened in the ABPP assay. Analytical runs were performed at 1, 20 and 100 μM probe concentrations applied to SH-SY5Y and A549 cells. Analysis by SDS-PAGE and fluorescence scanning revealed the most intense reactivity profile for probe **9** (Figure 2).[47]Also showing specific labeling, but to a lesser degree, were probes **8**, and the C1- and C3-propargyl oximes **4** and then **6**. As proof of concept, the 'inert' saturated probes **5** and **7** did not show any specific labeling in these assays, serving as a support for the pharmacological hypothesis for the mode of action of WitA. These results nicely correlate with the expected chemical reactivity of each probe, as the unsaturated oxime of probe **4** is not only less electrophilic than the corresponding enones of probes **8** and **9**, but possible steric congestion within the binding pocket of the targets with the propargylic oxime group at the C1-position could very well explain the less specific labeling observed for probe **4** over probes **8** and **9**.

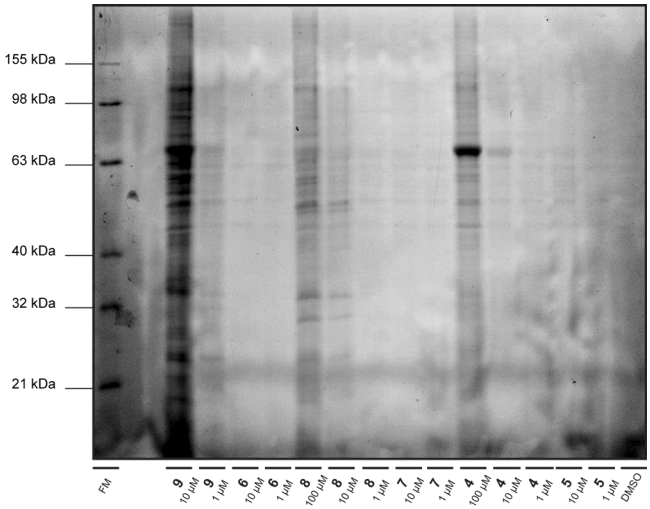

Figure 2. Representative SDS-PAGE showing analytical labeling of cytosol fraction of SH-SY5Y cells incubated with all six WitA probes (at a 1, 10 or 100 μM concentration) for 6 hours in PBS at 0.1% DMSO. Fluorescent marker (FM) lane designates protein size in kDa. No bands were found for the membrane fractions (data not shown)

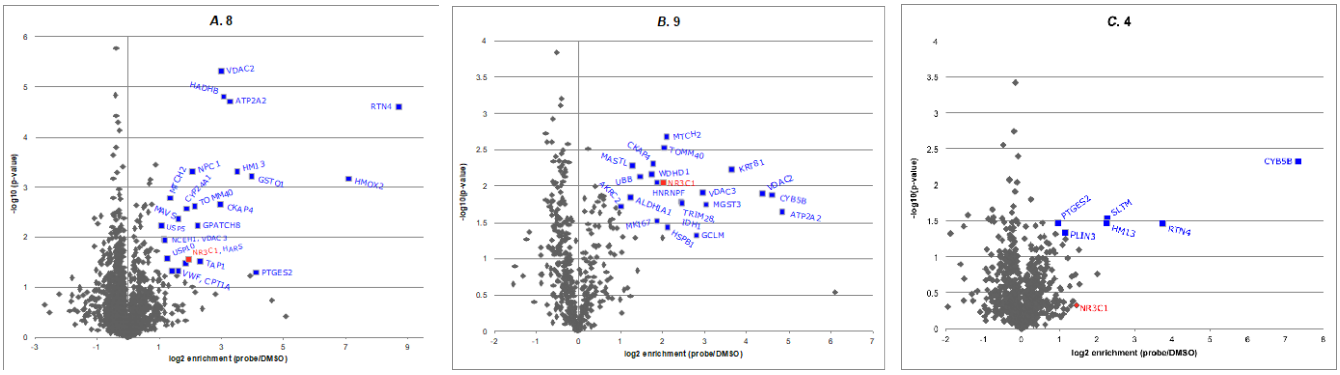

Figure 3. SILAC data volcano plots of WitA probes **8** (A), **9** (B) and **4** (C): fold-change, enrichment extent normalized to the DMSO control (log_2 enrichment) versus statistical significance ($-log_{10}$ p-value); p-value from ANOVA statistical model; top hits designated in blue and labeled, GR (NR3C1) is labeled in red. Targets in common ranked according to enrichment and p-value are displayed in Table 1.

Table 1. Targets in Common from Activity-Based Profiling with WitA Probes **4**, **8**, and **9**.

Rank	protein names	gene names	probe hit
1	sarcoplasmic/endoplasmic reticulum calcium ATPase 2	ATP2A2	**8**, **9**
2	voltage-dependent anion-selective channel protein 2	VDAC2	**8**, **9**
3	reticulon-4	RTN4	**4**, **8**, **9**
4	cytochrome b5 type B	CYB5B	**4**, **8**, **9**
5	cytoskeleton-associated protein 4	CKAP4	**4**, **8**, **9**
6	microsomal glutathione S-transferase 3	MGST3	**4**, **8**, **9**
7	minor histocompatibility antigen H13	HM13	**4**, **8**
8	mitochondrial import receptor subunit TOM40 homolog	TOMM 40	**8**, **9**
9	glutathione S-transferase omega-1	GSTO1	**8**, **9**
10	mitochondrial carrier homolog 2	MTCH2	**8**, **9**
11	glucocorticoid receptor	NR3C1	**4**, **8**, **9**
12	1,25-dihydroxyvitamin D(3) 24-hydroxylase, mitochondrial	CYP24 A1	**4**, **8**
13	voltage-dependent anion-selective channel protei 3	VDAC3	**8**, **9**
14	prostaglandin E synthase 2	PTGES 2	**4**, **8**
15	histidine-tRNA ligase, cytoplasmic	HARS	**4**, **8**

In order to elucidate the identity of all targets, quantitative, gel-free ABPP was performed via stable isotope labeling of amino acids in cell culture (SILAC) with the top three probes exhibiting the most pronounced labeling effect from the analytical experiments.[48] A549 cells were cultivated in media containing either heavy or light isotope labeled amino acids. These cells were then treated with the probes **4**, **8** or **9** at 10 μM concentration (or DMSO control). The cells were then lysed, pooled with the control, clicked to a biotin-azide linker[49] and enriched using avidin beads. The enriched proteins were digested using trypsin. The resulting solution was analyzed by high-resolution liquid chromatography tandem MS (LC-MS/MS). Log_2(isotopic ratios) values of zero indicate no enrichment as compared to the DMSO control, and ratios greater than 1-fold with a p-value of <0.05 were regarded as significant hits. These top hits with our three active probes are depicted in the upper right hand area of the corresponding volcano plots (A-C, Figure 3).[50] In addition, the hits shared *in common* between the three probes were identified and ranked according to enrichment and p-value to give the 15 hits listed in Table 1 (Figure 3).[51]

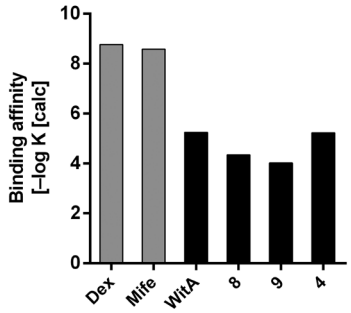

Figure 4. Predicted GR binding affinities [–log(K_{calc})] of compounds of interest calculated using *VirtualToxLab*.

While several of these hits might be of interest in understanding neurological pathways, we were particularly interested in the glucocorticoid receptor (GR, systematic name: NR3C1). The GR is a 78.7 kDa protein that belongs to the family of nuclear receptors and regulates genes for development, metabolism and immune response, through either transactivation or transrepression mechanisms.[52-54] Molecules that modulate this target, *i.e.* glucocorticoids, are mediators of stress response. A 2014 report by Terada and co-workers found that an antagonist of GR, such as mifepristone (RU486, Mife, **3**, Figure 1), can induce neurite outgrowth by phosphorylation of Akt (protein kinase B, PKB) and extracellular regulated kinase 1/2 (ERK1/2), which are involved downstream in nerve growth factor (NGF)-induced neurite outgrowth.[55] At the same time, GR agonists like dexamethasone (Dex, **2**, Figure 1) impair neurite outgrowth through interference of activation/phosphorylation of these same targets. In addition, treatment with Mife reversed the inhibitory activity of Dex on neurite outgrowth via the same NGF-induced Akt and ERK1/2 phosphorylation pathways. Mife has been previously demonstrated to reverse effects of glucocorticoid (GC) treatment and restore neurogenesis in cells,[56-58] and has become associated with neuroprotection,[59-62] implying that this is a glucocorticoid-dependent process.[63] It is also known that GCs exacerbate clinical symptoms and neurodegenerative processes (*in vivo* and *in vitro*),[64] and that GR-mediated transrepression has been linked to prevent neurodegeneration in Huntington's disease.[65] Therefore, the present study investigated whether the WitA-dependent effect on neurite outgrowth might be mediated by GR.

2.4 Computational approaches

We initiated our investigation of a potential binding of WitA to GR with the computational modeling program *VirtualToxLab*,[65] an *in silico* anti-target screening tool.[66-67,68] This technology is based on an automated, flexible docking calculation combined with multi-dimensional quantitative structure–activity relationship (QSAR) protocol that simulates and quantifies the binding of small molecules towards a series of currently 16 proteins, known or suspected to trigger adverse effects: 10 nuclear receptors (androgen receptor, estrogen receptor α, estrogen receptor β, GR, liver X receptor, mineralocorticoid receptor, peroxisome proliferator-activated receptor γ, progesterone receptor, thyroid receptor α, thyroid receptor β), four members of the cytochrome P450 enzyme family (CYP1A2, CYP2C9, CYP2D6, CYP3A4), a cytosolic transcription factor (aryl hydrocarbon receptor) and a potassium ion channel (hERG). While binding modes and affinities were predicted towards all 16 target proteins comprising the *VirtualToxLab*, the interest was mainly focused on GR.[69] GR agonist Dex was predicted to bind with 1.7 nM affinity to GR (exp. = 2.0 nM), while the predicted affinity of the known GR antagonist Mife was 2.6 nM (exp. = 15 nM) (Figure 4). For WitA, a weaker affinity of 5.7 μM for GR was predicted, and the ABPP-active WitA probes were predicted to bind with similar or lower affinity than WitA. Affinities computed with the *VirtualToxLab* represent a "thermodynamic" estimate only and do not account for the kinetic stability of the ligand–protein complex. To address this issue, WitA was probed further through iterative inspection in real-time 3D by molecular dynamics (MD) simulations, which could require correcting the "thermodynamic affinity" in either direction. Both Dex and WitA demonstrated stable ligand–protein interactions throughout the entire 100 ns MD simulation.[70] Each complex was further stabilized by the dynamic relaxation of the technique, indicating that the "thermodynamic" binding affinities might be slightly higher than those predicted by the *VirtualToxLab*.

2.5 Neurite outgrowth GR competition assays

We then wanted to clarify if WitA's neurite outgrowth activity was linked to its ability to modulate GR. Therefore, we performed *in vitro* neurite outgrowth experiments with Dex, Mife, and WitA. Human neuroblastoma SH-SY5Y cells were cultured in DMEM/F-12 media supplemented with 10% fetal bovine serum and 1% penicillin-streptomycin at 37°C in a humidified atmosphere (5% CO_2 content). For neurite outgrowth experiments the cells were seeded on collagen-coated 24-well plates and treated with 1 μM of the corresponding compounds, vehicle control (0.1% DMSO) or

all-*trans* retinoic acid (ATRA, RA) as a positive control. After a 6-day incubation, the media was removed and cells were fixed with a 4% buffered formaldehyde solution and stained with modified Giemsa stain to visualize the cell bodies for subsequent imaging under a phase-contrast microscope. All assays were performed in triplicate, with 6–11 images randomly taken between biological replicates, and at least 350 cells counted per treatment per plate (three wells/plate per treatment). Cells having at least one neurite with a length of more than 50 μm were counted as differentiated (positive). The ratio of neurite positive cells to total cells was calculated and error is represented by the standard error of the mean (SEM).

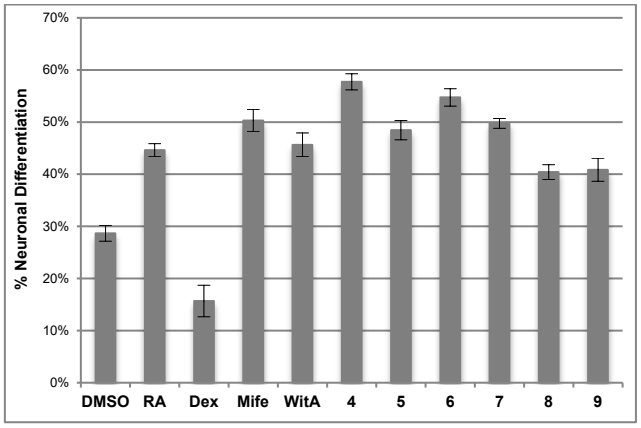

Figure 6. Neurite outgrowth of human SH-SY5Y cells treated with WitA (**1**), Dex (**2**), Mife (**3**), and WitA probes (**4**–**9**). 0.1% DMSO and RA are vehicle and positive controls. Data represents mean ± SEM from three independent experiments in triplicates For statistical analysis, ANOVA and post hoc tests (Dunnett's Method and Tukey Kramer Method) were used.[77]

From these experiments, we observed that all six withanolide probes induced neurite outgrowth of SHSY5Y cells (Figure 6). All four oxime probes (**4**–**7**) induced outgrowth to a similar extent as WitA and Mife and showed significantly higher activity than propargyl ester probes **8** and **9**.[72] Nevertheless, the propargyl esters still showed outgrowth activity comparable to the RA positive control. Moreover, WitA was also able to counteract the neurite outgrowth inhibition of Dex, suggesting that WitA is potentially acting as a GR antagonist, similar to Mife (Figure 7). The same effect was observed for both propargyl ester probes **8** and **9**. Interestingly, impaired neurite outgrowth was observed in the simultaneous treatments of both Dex and Mife with unsaturated C1 propargyl oxime **4**, within the statistical significance of the vehicle DMSO control (indicating no outgrowth).

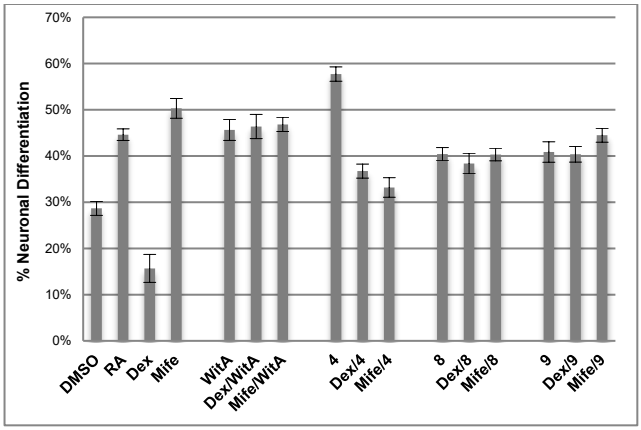

Figure 7. Neurite outgrowth in GR competition experiment of WitA (**1**), probes (**4**, **8**, **9**) with Dex (**2**) and Mife (**3**) in human SH-SY5Y cells. 0.1% DMSO and RA are vehicle and positive controls. Data represents mean ± SEM from three independent experiments in triplicates For statistical analysis, ANOVA and post hoc tests (Dunnett's Method and Tukey Kramer Method) were used.[79]

2.6 GR and MR transactivation bioassays

We then performed *in vitro* assays to investigate whether WitA might act as an antagonist of GR activity. HEK-293 cells were transiently transfected with human GR under the control of a GR sensitive luciferase promoter (Figure 8A). Additionally, the closely related mineralocorticoid receptor (MR) was tested for modulation by WitA (Figure 8B). 10 μM WitA was not able to stimulate GR-mediated activation of the luciferase reporter gene, whereas the MR was weakly activated. However, and more importantly regarding GR-dependent neuronal outgrowth, no antagonistic effect on the cortisol-dependent GR activation could be observed with 1 μM WitA. In addition, neither an agonistic nor an antagonistic activity of WitA on MR function could be observed. Thus, a direct interference of WitA with the GR and the MR could not be demonstrated within this cell-based assays.

To exclude the possibility that either WitA is under the control of efflux transport or that it was unable to cross the cell membrane, a GR binding assay was performed under cell-free conditions. Lysates of SF9 cells expressing recombinant human GR were incubated in the presence of 10 nM ^{3}H-dexamethasone as a tracer and the unlabeled competitor (either 10 μM Dex or 1 or 10 μM WitA) until the binding equilibrium was reached. The GR bound fraction of ^{3}H-dexamethasone is displayed in Fig. 9. Unlike with unlabeled Dex, WitA could not displace ^{3}H-Dex from the GR binding site at concentrations up to 10 μM (Figure 9). This indicates that WitA is not a ligand for GR, as could be predicted by the calculated binding affinities of WitA, discussed above. These results are also in line with those from the transactivation assays, indicating that WitA does not induce neurite outgrowth by direct antagonism of GR.

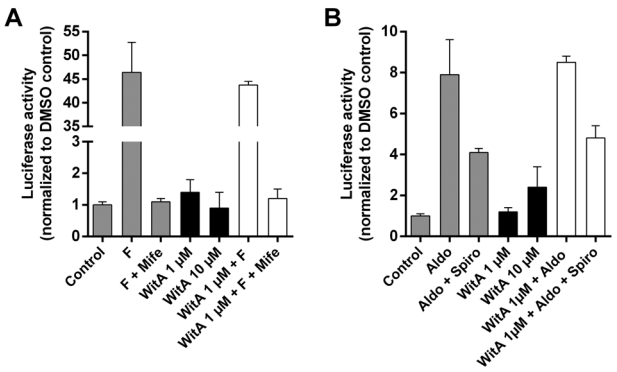

Figure 8. Effect of WitA on the modulation of GR and MR. Impact of WitA on GR (A) and MR (B) transactivation in HEK-293 cells transfected with a corticosteroid receptor sensitive luciferase reporter gene and human GR or human MR. Cells were incubated for 24 h in the presence or absence of 100 nM cortisol (F) or 1 µM Mife for GR, and 10 nM aldosterone (Aldo) or 1 µM spironolactone (Spiro) for MR. WitA was added at 1 or 10 µM. Data were normalized to vehicle control (0.05% DMSO) and represent mean ± SD from a representative experiment performed in triplicates.

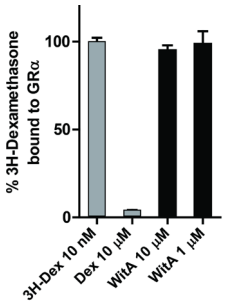

Figure 9. Displacement of radiolabeled Dex from GR with unlabeled competitor (WitA or Dex). Values were normalized to the maximal binding activity of 10 nM ^{3}H-Dex.

2.7 GR docking study

To computationally rationalize the results obtained from the transactivation and binding assays, docking studies comparing WitA and Dex for important binding interactions in the GR binding pocket were conducted using the same crystal structure as in the *VirtualToxLab* screening (PDB code 1M2Z. Figure 10A illustrates docked Dex (grey) and WitA (purple) in the GR binding site. The automatically generated pharmacophore interaction pattern revealed different residues forming hydrophobic and hydrogen bond (H-bond) interactions for Dex (Figure 10B) and WitA (Figure 10C). Generally, the docking calculations displayed different conformations for WitA, whereas Dex was found to fit in one major pose. Dex is stabilized by H-bond interactions in the GR binding pocket, exerted by oxygen and nitrogen atoms of the following residues: Asn564, Gln570, Arg611, Gln642 and Thr739. These interactions are known to be important for GR activation.[80] However, the H-bond interactions of Wit A with the GR adopt clearly greater distances and two of five hydrogen bonds involve a sulfur center (Met601 and Cys736). These interactions are generally regarded as weak H-bonds compared to interactions including oxygen or nitrogen groups. Furthermore, WitA has less hydrophobic interaction partners than Dex. Although we were able to dock WitA into the binding pocket of GR and therefore confirmed the *VirtualToxLab* screening results, the interaction pattern shows distinctively less favorable interactions compared to Dex. This may explain the inability of WitA to displace Dex from GR in the lysate binding assay. A weak but covalent binding of WitA to GR might be missed by the docking calculations; however, *in vitro* verification assessments excluded this possibility. Nevertheless, regarding its effect on neurite outgrowth, one would expect an antagonistic action of WitA on GR function. In contrast to the agonist bound position, active antagonist conformations can displace the helix 12 and thereby trigger a molecular shift to alter the coactivator site into the corepressor site.[81] Docking of WitA into a GR X-ray structure with Mife as co-crystallized ligand (PDB code 1NHZ) showed no interference of WitA with the helix 12 (data not shown). Thus, the molecular modeling does not support a direct antagonistic activity of WitA on GR, in line with the lack of antagonistic activity of WitA in the transactivation assay.

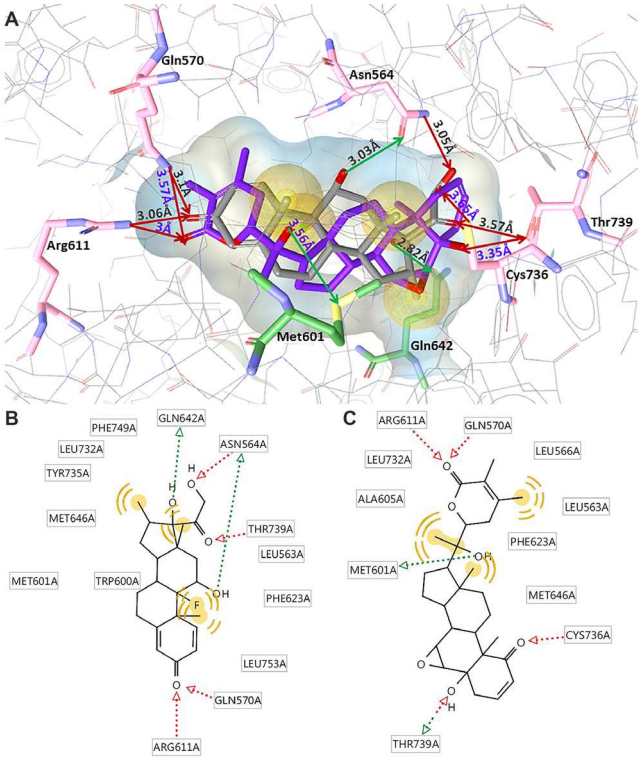

Figure 10. Docking of Dex and WitA into the binding pocket of GR. (A) Dex (grey) and WitA (purple) docked into the GR binding site. Amino acid residues important for binding are depicted as sticks. Yellow spheres display H-bond features important for binding. Arrows indicate H-bonds with the corresponding distance between the ligand and the residue of the binding pocket (grey numbering belong to Dex and purple to WitA). The color code of the arrows correspond with binding

interactions of part B and C. (B) Two-dimensional representation of the binding interactions of Dex with GR. (C) Binding interactions of WitA and GR are shown. Hydrophobic interactions are depicted in yellow, hydrogen bond acceptors in red and hydrogen bond donors in green.

3. Conclusion

In this study, we investigated the GR as a target for WitA–dependent neurite outgrowth activity. While results from target profiling, *VirtualToxLab* screening and *in vitro* GR competition neurite outgrowth assays supported this GR hypothesis, additional GR transactivation and binding assays and further docking studies did not support a direct interaction of WitA as GR antagonist causing the neurite outgrowth effect. However, we did confirm that WitA is able to reverse the neurite outgrowth inhibitory activity of Dex, similar to GR antagonist Mife. Nevertheless, a GR indirect effect of WitA by interfering with GR-related targets such as ERK, Akt, NF-κB, TRα, or Hsp90 might be possible. It is possible that WitA affects additional targets via a reversible binding mode, which we could not detect with the current ABPP design and would require the incorporation of photoreactive groups. Interactions have been already established between these targets and Mife, withanolide extract or withaferin A, and it is possible that we identified GR as a positive hit for WitA in our pulldown assay when WitA was actually modulating one of these targets instead of GR directly. [24, 54, 58, 60, 76-86] Ongoing efforts are being made to assess a potential connection through these targets. In addition, we are pursuing additional studies to follow-up on the other 14 proteins-of-interest, identified in our ABPP profiling study.

4. Experimental

4.1. General

Commercial reagents and solvents were purchased from Sigma-Aldrich, Alfa Aesar, Fisher Scientific, Acros Organics, or Fluorochem and used as received, unless otherwise noted. Deuterated solvents were purchased from Cambridge Isotope Laboratories, Inc. (Andover, MA, USA). Flash chromatography was carried out on Silicycle 60 Å silica gel (40–63 μm, 230–400 mesh. Eluents and R_f's are indicated. Analytical thin layer chromatography was performed using Merck silica gel 60 F254 plates (0.25mm thickness) and was visualized by UV light and fluorescent indicator, with or without heating (potassium permanganate, p-anisaldehyde or aqueous ceric ammonium molybdate stain).

All ^{1}H spectra were recorded on a Bruker Avance III 400MHz (400 MHz for ^{1}H and 101 MHz for ^{13}C) or Bruker Avance III 500MHz spectrometer (500 MHz for ^{1}H and 126 MHz for ^{13}C). Chemical shifts (δ-values) are reported in parts per million (ppm) relative to $CDCl_3$ (7.26 ppm for ^{1}H NMR and 77.0 ppm for ^{13}C NMR). ^{1}H NMR spectra are tabulated in the order: chemical shift, multiplicity, coupling constant (*J* in Hz), number of protons. Multiplicity is reported as follows: s = singlet, d = doublet, t = triplet, q = quartet, m = multiplet or unresolved; ap = apparent, br = broad.

Infrared spectra were recorded on a Varian 800 FT-IR ATR spectrophotometer and values are reported as frequency of absorptions in cm^{-1}. All HRMS-ESI spectra were recorded by the mass spectrometry service of the chemistry department at the University of Basel on a QTOF-ESI spectrophotometer (bruker MaXis 4G). Fragment ions are given in m/z with relative intensities (%) in parentheses. Melting points (m. p.) were collected on a Büchi B-545 apparatus in open capillaries. Optical rotations were measured on a Jasco P-2000 digital polarimeter with a sodium lamp (D-589 nm) in a 1 dm cylindrical cell (1 mL cell volume) and are reported as follows: $[\alpha]_\lambda^{T^\circ C}$ (c = g/100 mL, solvent).

4.2. Isolation of withanolide A

Powdered Ashwagandha root[93] (5 × 100 g + 10 × 250 g, purchased from Yoga Vidya, Horn-Bad Meinberg, Germany) was stirred in 500 g batches in a covered 2 L Erlenmeyer flask with 1.25 L of methanol overnight. The brown slurry was then transferred to a 10 cm diameter column with an additional 100 mL of methanol to rinse. The MeOH extract was allowed to percolate out (drip out by gravity) and was collected (~2 h). An additional 650 mL of methanol was added to the column, and allowed to percolate further (~3 h). The methanol remaining in the wet root powder was flushed out using nitrogen flow. The extract was carefully concentrated in vacuo. This procedure was repeated five times, until extract was obtained for all 3 kg of the Ashwangandha root.

The combined methanol extract (combined volume of ~1.5 L) was washed with pentane (3 × 500 mL) to remove grease and other apolar compounds, and was then carefully concentrated in vacuo to afford a thick, brown oil. To remove the more polar substances, this oil was taken up in EtOAc (500 mL), the organic layer was separated and the aqueous layer was washed 2 more times with EtOAc (200 mL). The combined EtOAc extracts were then washed with H_2O (3 × 500 mL), dried over Na_2SO_4, filtered and concentrated in vacuo to afford 17.4 g of a brown oil. All aqueous extracts were checked for withanolide A by TLC to make sure none was still present before disposal.

The crude oil was purified by flash column chromatography (FCC, wet load) with 70% to 100% EtOAc/pentanes, and then 5% and 20% MeOH/EtOAc, to afford 5.68 g of a yellow solid (collected during 80-100% EtOAc/pentane and 5% MeOH/EtOAc eluents). This solid was purified again by FCC with 40:1 DCM:MeOH to afford 2.1g of a yellow/white solid, which was then triturated with cold ether to afford 1.6 g of a white solid. A series of additional columns with 100X-250X silica gel, with either 8:1:1 EtOAc:$CHCl_3$:Hexane (dry load), or 40:1 DCM:MeOH (dry load), or 80% EtOAc/Hex (wet load with $CHCl_3$) as eluents. A total of 1.03 g of pure Withanolide A was obtained as white solid, as shown in Figure S1 in 0.038% yield (see supporting information). Also noteworthy, approximately 200 mg of Withanolide B (**S1**), or C20-dehydroxywithanolide A, was obtained as a white solid; WitB R_f = 0.65 (8:1:1 EtOAc/hexane/$CHCl_3$).[94] Analytical data of Withanolide A (**1**): $[\boldsymbol{\alpha}]_{\boldsymbol{D}}^{\boldsymbol{25^\circ C}}$ = +87.9° (c = 0.21, $CHCl_3$) [Lit: +86.8 when c = 1.15, $CHCl_3$]. **IR** (film) $\tilde{\nu}$ = 3437, 2984, 2937, 1703, 1679, 1446, 1374, 1295, 1220, 1188, 1137, 1099, 1073, 1028, 955, 909, 883, 815, 800, 727, 648, 612 cm^{-1}. **^{1}H NMR** (400 MHz, $CDCl_3$) δ 6.59 (ddd, *J* = 10.1, 5.2, 2.2 Hz, 1H), 5.85 (ddd, *J* = 10.1, 3.0,

1.0 Hz, 1H), 4.21 (dd, *J* = 13.4, 3.5 Hz, 1H), 3.32 (dd, *J* = 4.0, 2.1 Hz, 1H), 3.12 (d, *J* = 1.5 Hz, 1H), 3.04 (d, *J* = 3.9 Hz, 1H), 2.79 – 2.65 (m, 2H), 2.52 (ddd, *J* = 18.8, 5.2, 1.0 Hz, 1H), 2.43 – 2.35 (m, 1H), 2.37 (d, *J* = 1.3 Hz, 1H), 2.14 – 1.98 (m, 3H), 1.96 (s, 3H), 1.89 (s, 3H), 1.86 – 1.80 (m, 1H), 1.78 (ddd, *J* = 10.6, 10.6, 2.2 Hz, 1H), 1.61 – 1.34 (m, 7H), 1.32 (s, 3H), 1.18 (s, 3H), 0.96 (s, 3H). **^{13}C NMR** (126 MHz, $CDCl_3$) δ 203.3, 166.2, 149.0, 139.8, 129.1, 122.2, 81.1, 75.2, 73.4, 57.5, 56.5, 54.6, 52.1, 51.1, 44.0, 40.5, 36.9, 35.7, 35.2, 31.8, 23.3, 21.9, 21.9, 21.2, 20.7, 14.9, 13.9, 12.6. **HRMS** (ESI): Exact mass cald for $C_{28}H_{39}O_6$ $[M+H]^+$, 471.3. Found 471.3. [95]

4.3. Syntheses of molecular probes 4–7

(μ4a*R*,4b*S*,6a*S*,7*S*,9a*S*,9b*S*,9c*S*,10a*S*,10b*R*)-7-((*R*)-1-((*R*)-4,5-dimethyl-6-oxo-3,6-dihydro-2*H*-pyran-2-yl)-1-hydroxyethyl)-10b-hydroxy-4a,6a-dimethylhexadecahydro-4*H*-cyclopenta[1,2]phenanthro[9,10-*b*]oxiren-4-one (**4**): withanolide A hydroxylamine **S2** was prepared according to a modified procedure (see supporting information for details).[96] Withanolide A hydroxylamine **S2** (10 mg, 0.021 mmol) was taken up in DMSO (100 μL, 0.2 M) in a round bottom flask with magnetic stir bar under argon. KOH pellets (4 mg, 0.062 mmol, 3 equiv.) were added and dissolved to give a milky yellow solution. Then, added propargyl bromide (10 μL, 0.062 mmol, 80% by weight in toluene, 3 equiv.) and the solution turned brown. The reaction stirred for 3 hours and then added 1M HCl solution. The reaction mixture was extracted with DCM (3×), and then dried the combined organic layers over Na_2SO_4, filtered and concentrated *in vacuo* to afford a yellow oil. The crude product was purified by flash column chromatography with silica gel (×200 by weight) and with 80:1 DCM:MeOH as the eluent to afford the C1 propargyl oxime as a clear oil (6.3 mg, 58% yield). Analytical data for **4**: **TLC** R_f = 0.67 (8:1:1 EtOAc/hexane/$CHCl_3$, CAM stain). $[\boldsymbol{\alpha}]_{\boldsymbol{D}}^{\boldsymbol{24°C}}$ = +171.5° (c = 0.275, $CHCl_3$) **IR** (film) $\tilde{\nu}$ = 3526, 3279, 2941, 2919, 2359, 2325, 2212, 2050, 1985, 1705, 1446, 1381, 1317, 1290, 1130, 1095, 1039, 1003, 906, 876, 825, 788, 651, 620 cm^{-1}. **^{1}H NMR** (400 MHz, $CDCl_3$) δ 6.67 (ddd, *J* = 10.3, 2.7, 1.1 Hz, 1H), 6.01 (ddd, *J* = 10.3, 4.7, 2.5 Hz, 1H), 4.64 (dd, *J* = 2.4, 1.1 Hz, 2H), 4.21 (dd, *J* = 13.3, 3.5, 1H), 3.31 (dd, *J* = 3.7, 2.0 Hz, 1H), 3.01 (d, *J* = 3.9 Hz, 1H), 2.96 (d, *J* = 2.6 Hz, 1H), 2.91 – 2.82 (m, 1H), 2.52 – 2.32 (m, 5H), 2.16 – 1.98 (m, 3H), 1.95 (s, 3H), 1.89 (s, 3H), 1.87 – 1.77 (m, 2H), 1.63 – 1.34 (m, 7H), 1.33 (s, 3H), 1.09 (s, 3H), 0.98 (s, 3H). **^{13}C NMR** (126 MHz, $CDCl_3$) δ 166.2, 159.2, 148.9, 131.4, 122.2, 118.3 81.2, 80.3, 75.3, 74.0, 71.4, 61.4, 57.5, 56.8, 54.6, 52.4, 45.5, 44.1, 40.6, 37.4 36.7, 35.4, 31.9, 23.4, 22.7, 22.0, 21.3, 20.7, 16.1, 14.0, 12.6. **HRMS** (ESI): Exact mass cald for $C_{31}H_{41}NO_6$ $[M+H]^+$, 524.3. Found 524.3.

General procedure A for oxime ethers 5–7

To a solution of ketone (1.0 equiv.) in pyridine (freshly distilled over KOH pellets, 1.0 equiv.) was added the *O*-propargylhydroxylamine hydrochloride (**S4**, 3.0 equiv, see supporting information for synthetic details of **S4**) in an oven-dried round-bottom flask with stir bar (equipped with oven-dried reflux condenser), and the mixture was heated at 70 °C for the indicated time. The solvent was then removed under high vacuum, and the resulting residue was dissolved in CH_2Cl_2. Saturated NH_4Cl (aqueous) solution was added and the aqueous phase was extracted with CH_2Cl_2 (3×). The combined organic phases were dried over Na_2SO_4, filtered and concentrated *in vacuo*. The crude product was purified by flash column chromatography under the indicated conditions to yield the oxime ethers **5**–**7**.

(*R*)-6-((*R*)-1-hydroxy-1-((4a*S*,4b*S*,6a*S*,7*S*,9a*S*,9b*S*,9c*S*,10a*S*,10b*R*,*E*)-10b-hydroxy-4a,6a-dimethyl-4-((prop-2-yn-1-yloxy)imino)hexadecahydro-1*H*-cyclopenta[1,2]phenanthro[9,10-*b*]oxiren-7-yl)ethyl)-3,4-dimethyl-5,6-dihydro-2*H*-pyran-2-one (**5**): saturated C1 propargyl oxime **5** was made according to general procedure A. The reaction was performed on 21 μmol scale of saturated withanolide A (**S3**, see supporting information for synthetic details) for 7 hours. Purification by flash column chromatography was performed with silica gel (150X by weight) with 120:1 CH_2Cl_2:MeOH as the eluent, and afforded **5** as a white solid in a 75% yield. Analytical data for **5**: **TLC** R_f = 0.64 (50% EtOAc/pentanes, CAM stain); [R_f (starting material **1**) = 0.49 (50% EtOAc/pentanes)]. **mp** = 200–202 °C. $[\boldsymbol{\alpha}]_{\boldsymbol{D}}^{\boldsymbol{24°C}}$ = +93.4° (c = 0.14, $CHCl_3$). **IR** (film) $\tilde{\nu}$ = 3267, 2944, 2361, 2338, 2166, 1703, 1441, 1384, 1314, 1291, 1178, 1133, 1095, 1041, 1002, 896, 761, 686, 631 cm^{-1}. **^{1}H NMR** (500 MHz, $CDCl_3$) δ 4.66 – 4.57 (m, 2H), 4.21 (dd, *J* = 13.4, 3.6 Hz, 1H), 3.30 – 3.22 (m, 2H), 2.99 (d, *J* = 4.0 Hz, 1H), 2.92 (s, 1H), 2.61 (dddd, *J* = 9.2, 2.9, 2.9, 2.9 Hz, 1H), 2.40 (dd, *J* = 2.4, 2.4 Hz, 1H), 2.39 – 2.32 (m, 2H), 2.11 (dd, *J* = 17.4, 2.9 Hz, 1H), 2.08 – 1.96 (m, 3H), 1.95 (s, 3H), 1.95 – 1.90 (m, 1H), 1.89 (s, 3H), 1.87 – 1.82 (m, 1H), 1.79 (ddd, *J* = 10.5, 10.5, 2.3 Hz, 1H), 1.75 – 1.33 (m, 8H), 1.32 (s, 3H), 1.21 – 1.13 (m, 1H), 1.11 (s, 3H), 0.96 (s, 3H). **^{13}C NMR** (101 MHz, $CDCl_3$) δ 166.3, 162.4, 149.0, 122.2, 81.2, 80.7, 75.3, 73.8, 72.5, 61.0, 57.6, 57.3, 54.5, 52.3, 47.3, 44.4, 40.6, 36.9, 35.3, 32.6, 31.9, 23.2, 22.1, 22.1, 21.3, 20.7, 20.4, 20.2, 16.2, 14.1, 12.6. **HRMS** (ESI): Exact mass cald for $C_{31}H_{44}NO_6$ $[M+H]^+$, 526.3. Found 526.3.

(4a*R*,4b*S*,6a*S*,7*S*,9a*S*,9b*S*,9c*S*,10a*S*,10b*R*)-7-((*R*)-1-((*R*)-4,5-dimethyl-6-oxo-3,6-dihydro-2*H*-pyran-2-yl)-1-hydroxyethyl)-10b-hydroxy-4a,6a-dimethyl-1,4a,4b,5,6,6a,7,8,9,9a,9b,9c,10a,10b-tetradecahydro-2*H*-cyclopenta[1,2]phenanthro[9,10-*b*]oxiren-2-one (**10**): C3 enone (**10**) was accessed through our previously published procedure[95b] from withanolide A (**1**) on a 0.21 mmol scale: through the epoxy ketone (**S5**, 88% yield) intermediate, and a Wharton transposition to allylic alcohol (**S6**, 65% yield). Then, powdered 4Å molecular sieves (200 mg, 40X by weight) were added to the solution of allylic alcohol **S6** (25 mg, 52.7 μmol) in CH_2Cl_2 (4 mL, 0.013 M) in an oven dried round bottom flask with magnetic stir bar. This mixture stirred for 5 minutes at room temperature under argon, when pyridinium dichromate (36 mg, 94.1 μmol, 1.8 equiv.) was added and the mixture stirred at room temperature for 2 hours and 20 minutes. The mixture was then filtered over a celite pad, washing with CH_2Cl_2. The combined organic layer was successively washed with 1 N HCl (2 × 30 mL,) and brine (60 mL), and then dried over Na_2SO_4, filtered and concentrated *in vacuo*. The crude material was purified by flash column chromatography (eluent: 80:1 CH_2Cl_2/MeOH) to obtain enone **10** (21.6 mg, 45.9 μmol, 87% yield) as a white solid.

Analytical data for **10**: **TLC** R_f = 0.5 (EtOAc). **mp** = 252–255 °C. $[\alpha]_D^{25°C}$ = +71.1° (c = 0.385, $CHCl_3$). **IR** (film) $\tilde{\nu}$ = 3394, 2984, 2946, 1693, 1658, 1471, 1385, 1321, 1296, 1269, 1187, 1182, 1136, 1116, 1064, 1019, 986, 916, 815, 762, 745 cm^{-1}. **^{1}H NMR** (500 MHz, $CDCl_3$) δ 6.97 (d, *J* = 10.3 Hz, 1H), 5.99 (dd, *J* = 10.2, 0.9 Hz, 1H), 4.21 (dd, *J* = 13.4, 3.5 Hz, 1H), 3.36 (dd, *J* = 3.9, 2.5 Hz, 1H), 3.16 (d, *J* = 2.0 Hz, 1H), 3.09 (d, *J* = 3.8 Hz, 1H), 2.85 (dd, *J* = 17.0, 2.1 Hz, 1H), 2.66 (dd, *J* = 17.0, 1.0 Hz, 1H), 2.45 – 2.32 (m, 2H), 2.25 – 1.97 (m, 3H), 1.96 (s, 3H), 1.89 (s, 3H), 1.88 – 1.81 (m, 2H), 1.72 – 1.34 (m, 8H), 1.32 (s, 3H), 1.16 (s, 3H), 0.98 (s, 3H). **^{13}C NMR** (126 MHz, $CDCl_3$) δ 196.8, 166.1, 153.1, 148.9, 128.1, 122.2, 81.1, 75.2, 72.1, 57.7, 56.7, 54.4, 51.7, 46.6, 44.3, 42.8, 40.1, 35.7, 35.3, 31.8, 23.1, 22.2, 21.3, 20.8, 20.7, 20.5, 13.9, 12.6. **HRMS** (ESI): Exact mass cald for $C_{28}H_{38}NaO_6$ $[M+Na]^+$, 493.3. Found 493.5.

(*R*)-6-((*R*)-1-hydroxy-1-((4a*R*,4b*S*,6a*S*,7*S*,9a*S*,9b*S*,9c*S*,10a*S*,10b*R*,*E*)-10b-hydroxy-4a,6a-dimethyl-2-((prop-2-yn-1-yloxy)imino)-2,4a,4b,5,6,6a,7,8,9,9a,9b,9c,10a,10b-tetradecahydro-1*H*-cyclopenta[1,2]phenanthro[9,10-*b*]oxiren-7-yl)ethyl)-3,4-dimethyl-5,6-dihydro-2*H*-pyran-2-one (**6**): C3 propargyl oxime **6** was made according to general procedure A. The reaction was performed on 12 μmol scale of enone **10**, with a reaction time of 3 days. Purification by flash column chromatography was performed with silica gel (1000X by weight) with 120:1 and then 80:1 CH_2Cl_2:MeOH as the eluent, and afforded (*E*)-**6** (4.6 mg, 8.8 μmol, 74% yield) as a white solid. If the reaction time was reduced to 4 hours, then both oxime diastereomers were obtained (86% yield of 1:1 *E*:*Z* ratio on 10 μmol scale of enone **10**). Only the (*E*)-**6** isomer was used in the biological studies. Analytical data for (*E*)-**6**: **TLC** R_f = 0.67 (50% EtOAc/pentanes or 8:1:1 EtOAc/hexane/$CHCl_3$, CAM stain). **mp** = 185-187 °C (decomposition). $[\alpha]_D^{25°C}$ = +81.4° (c = 0.5, $CHCl_3$). **IR** (film) $\tilde{\nu}$ = 3518, 3303, 2939, 2360, 1703, 1461, 1386, 1319, 1287, 1132, 1099, 1043, 1007, 914, 731, 682, 648 cm^{-1}. **^{1}H NMR** (400 MHz, $CDCl_3$) δ 6.27 (d, *J* = 10.2 Hz, 1H), 6.18 (d, *J* = 10.1 Hz, 1H), 4.71 (d, *J* = 2.4 Hz, 2H), 4.20 (dd, *J* = 13.3, 3.4 Hz, 1H), 3.33 (dd, *J* = 2.9, 2.9 Hz, 1H), 3.18 – 3.08 (m, 2H), 3.04 (s, 1H), 2.63 (d, *J* = 17.7 Hz, 1H), 2.49 (dd, *J* = 2.4, 2.4 Hz, 1H), 2.43-2.33 (m, 2H), 2.19 – 1.99 (m, 3H), 1.95 (s, 3H), 1.89 (s, 3H), 1.86 – 1.78 (m, 2H), 1.68 – 1.55 (m, 3H), 1.50 – 1.37 (m, 4H), 1.31 (s, 3H), 0.98 (s, 3H), 0.96 (s, 3H). **^{13}C NMR** (101 MHz, $CDCl_3$) δ 166.1, 154.4, 148.9, 140.1, 122.9, 122.2, 81.1, 77.4, 75.2, 74.7, 69.4, 61.8, 57.7, 57.1, 54.4, 51.8, 44.3, 42.1, 40.2, 35.9, 35.2, 33.6, 31.8, 23.1, 22.2, 21.3, 20.7, 20.7, 20.5, 13.8, 12.6. **HRMS** (ESI): Exact mass cald for $C_{31}H_{42}NO_6$ $[M+H]^+$, 524.3. Found 524.3.

Analytical data for (*Z*)-**6**: Also isolated as a white solid. **TLC** R_f = 0.58 (50% EtOAc/pentanes or 8:1:1 EtOAc/hexane/$CHCl_3$, CAM stain). **mp** = 118-120 °C. $[\alpha]_D^{25°C}$ = +75.6° (c = 0.34, $CHCl_3$). **IR** (film) $\tilde{\nu}$ = 3521, 3295, 2929, 2362, 2340, 1704, 1461, 1427, 1383, 1319, 1288, 1133, 1099, 1043, 1007, 972, 917, 816, 763, 731, 647 cm^{-1}. **^{1}H NMR** (400 MHz, $CDCl_3$) δ 6.75 (d, *J* = 10.3 Hz, 1H), 6.30 (d, *J* = 10.4 Hz, 1H), 4.68 (dd, *J* = 2.4, 1.0, 2H), 4.20 (dd, *J* = 13.4, 3.5 Hz, 1H), 3.33 (dd, *J* = 3.1, 1H), 3.14 – 3.05 (m, 2H), 2.84 (d, *J* = 16.2 Hz, 1H), 2.66 (d, *J* = 16.0 Hz, 1H), 2.46 (dd, *J* = 2.4 Hz, 1H), 2.44 – 2.33 (m, 2H), 2.20 – 2.10 (m, 3H), 1.95 (s, 3H), 1.89 (s, 3H), 1.87 – 1.75 (m, 2H), 1.69 – 1.55 (m, 2H), 1.52 – 1.35 (m, 6H), 1.32 (s, 3H), 1.02 (s, 3H), 0.96 (s, 3H). **^{13}C NMR** (126 MHz, $CDCl_3$) δ 166.1, 151.4, 148.9, 143.0, 122.2, 115.9, 81.1, 80.1, 75.2, 74.4, 70.1, 61.5, 57.6, 57.0, 54.4, 51.7, 44.3, 42.8, 40.1, 36.9, 35.9, 35.3, 31.8, 29.8, 23.1, 22.2, 21.2, 20.9, 20.7, 20.7, 13.8, 12.6. **HRMS** (ESI): Exact mass cald for $C_{31}H_{42}NO_6$ $[M+H]^+$, 524.3. Found 524.4.

(*R*)-6-((*R*)-1-hydroxy-1-((4a*R*,4b*S*,6a*S*,7*S*,9a*S*,9b*S*,9c*S*,10a*S*,10b*R*,*Z*)-10b-hydroxy-4a,6a-dimethyl-2-((prop-2-yn-1-yloxy)imino)hexadecahydro-1*H*-cyclopenta[1,2]phenanthro[9,10-*b*]oxiren-7-yl)ethyl)-3,4-dimethyl-5,6-dihydro-2*H*-pyran-2-one (**7**): Saturated C3 propargyl oxime **7** was made according to general procedure A. The reaction was performed on 8 μmol scale of ketone **S7** (for details of **S7**, see supporting information), with a reaction time of 5 hours. The 3:2 ratio of *Z*:*E* isomers could be separated by flash column chromatography purification with silica gel (1000X by weight) with 120:1 and then 80:1 CH_2Cl_2:MeOH as the eluent. Saturated C3 propargyl oxime **7** (4.1 mg, 7.8 μmol, >99% yield) was obtained as a white solid. Only the (*E*)-**7** isomer was used in the biological studies. Analytical data for (*Z*)-**7**: **TLC** R_f = 0.55 (50% EtOAc/pentanes, CAM stain). **mp** = 200-204 °C (decomposition). $[\alpha]_D^{24°C}$ = +65.6° (c = 0.25, $CHCl_3$). **IR** (film) $\tilde{\nu}$ = 3531, 3287, 2943, 2361, 2338, 2111, 2051, 1985, 1705, 1462, 1425, 1335, 1319, 1287, 1181, 1133, 1098, 1047, 1006, 896, 858, 784, 735, 631 cm^{-1}. **^{1}H NMR** (400 MHz, $CDCl_3$) δ 4.72 – 4.58 (m, 2H), 4.20 (dd, *J* = 13.3, 3.5 Hz, 1H), 3.33 – 3.26 (m, 1H), 3.20 (d, *J* = 15.6 Hz, 1H), 3.01 (d, *J* = 3.8 Hz, 1H), 2.86 (d, *J* = 2.1 Hz, 1H), 2.54 – 2.41 (m, 1H), 2.45 (dd, *J* = 2.4, 2.4 Hz, 1H), 2.40 – 2.31 (m, 3H), 2.28 (dd, *J* = 15.7, 2.1 Hz, 1H), 2.15 – 1.98 (m, 3H), 1.95 (s, 3H), 1.89 (s, 3H), 1.86 – 1.64 (m, 3H), 1.62 – 1.53 (m, 1H), 1.48 (dd, *J* = 9.8, 9.8 Hz, 1H), 1.41 – 1.32 (m, 4H), 1.30 (s, 3H), 1.28 – 1.23 (m, 2H), 1.17 – 1.06 (m, 1H), 0.93 (s, 3H), 0.88 (s, 3H). **^{13}C NMR** (101 MHz, $CDCl_3$) δ 166.1, 158.7, 148.9, 122.2, 81.1, 80.3, 75.2, 74.2, 70.5, 61.1, 58.0, 57.8, 54.5, 51.8, 44.2, 40.2, 38.5, 38.4, 34.9, 33.8, 31.8, 28.8, 26.4, 23.2, 22.2, 21.2, 20.7, 20.3, 15.2, 13.8, 12.6. **HRMS** (ESI): Exact mass cald for $C_{31}H_{44}NO_6$ $[M+H]^+$, 526.3. Found 526.3.

Analytical data for (*E*)-**7**: **TLC** R_f = 0.46 (50% EtOAc/pentanes, CAM stain). **mp** = 199–202 °C (decomposition). $[\alpha]_D^{24°C}$ = +36.7° (c = 0.15, $CHCl_3$). **IR** (film) $\tilde{\nu}$ = 2938, 2361, 2341, 2115, 2048, 1985, 1705, 1458, 1425, 1385, 1319, 1290, 1183, 1099, 1046, 1008, 895, 760, 732, 685, 631 cm^{-1}. **^{1}H NMR** (400 MHz, $CDCl_3$) δ 4.71 – 4.59 (m, 2H), 4.20 (dd, *J* = 13.3, 3.5 Hz, 1H), 3.29 (dd, *J* = 3.9, 2.2 Hz, 1H), 3.18 (dd, *J* = 17.1, 6.1 Hz, 1H), 2.98 (d, *J* = 3.8 Hz, 1H), 2.86 (d, *J* = 1.9 Hz, 1H), 2.56 – 2.32 (m, 5H), 2.16 – 1.99 (m, 4H), 1.95 (s, 3H), 1.89 (s, 3H), 1.88 – 1.73 (m, 2H), 1.66 – 1.53 (m, 2H), 1.49 (dd, *J* = 9.6, 9.6 Hz, 1H), 1.44 – 1.34 (m, 2H), 1.30 (s, 3H), 1.27– 1.19 (m, 2H), 1.16 – 1.07 (m, 1H), 0.93 (s, 3H), 0.89 (s, 3H). **^{13}C NMR** (101 MHz, $CDCl_3$) δ 166.1, 158.4, 148.9, 122.2, 81.1, 80.3, 75.2, 74.2, 70.4, 61.1, 57.9, 57.6, 54.5, 51.8, 44.2, 40.2, 38.9, 38.4, 38.3, 34.9, 31.8, 27.9, 23.2, 22.2,

21.2, 20.7, 20.6, 20.4, 14.9, 13.8, 12.6. **HRMS** (ESI): Exact mass cald for $C_{31}H_{44}NO_6$ $[M+H]^+$, 526.3. Found 526.3.

4.4. Syntheses of molecular probes 8–9

prop-2-yn-1-yl (*S*,2*Z*,4*E*)-6-hydroxy-6-((4a*R*,4b*S*,6a*S*,7*S*,9a*S*,9b*S*,9c*S*,10a*S*,10b*R*)-10b-hydroxy-4a,6a-dimethyl-4-oxo-4,4a,4b,5,6,6a,7,8,9,9a,9b,9c,10a,10b-tetradecahydro-1*H*-cyclopenta[1,2]phenanthro[9,10-*b*]oxiren-7-yl)-2,3-dimethylhepta-2,4-dienoate (**8**): To a solution of withanolide A (**1**, 30 mg, 0.063 mmol) dissolved in CH_2Cl_2 (anhydrous, 7 mL, 0.009 M) in a round bottom flask with stir bar at room temperature was added *n*Bu_4NI (3 mg, 0.006 mmol, 0.1 equiv.), a 50% NaOH solution (3.5 g in 7 mL H_2O, 0.009 M) and then the propargyl bromide (8 µL, 0.070 mmol, 1.1 equiv.). The faint yellow reaction stirred for 3 days. Then, added 5 mL of sat. NH_4Cl solution (aq.) and brought the mixture to pH of 7 with conc. HCl and 2M HCl. The aqueous layer was extracted with EtOAc (3×). The combined organic layers were washed with brine (1×), dried over $MgSO_4$, filtered and concentrated *in vacuo* to afford a yellow oil. This was then purified by flash column chromatography with silica gel (×200) with 20, 30 and 40% EtOAc/pentanes as the eluent. Collected the unsaturated propargyl ester **9** (1.4 mg, 5% yield) as a yellow oil, propargyl ester **8** (10.6 mg, 33% yield) as a white solid, and starting material (8.4 mg, 28% mass recovery of **1**).

Analytical data for **8**: **TLC** R_f = 0.44 (50% EtOAc/pentanes, CAM stain). **mp** = 156-158 °C. $[\alpha]_D^{25°C}$ = –6.5° (c = 0.265, $CHCl_3$). **IR** (film) $\tilde{\nu}$ = 3730, 3592, 3485, 3271, 2927, 2874, 2851, 2361, 2340, 2198, 2166, 1687, 1456, 1383, 1291, 1262, 1215, 1105, 1033, 975, 906, 785, 630 cm^{-1}. **^{1}H NMR** (400 MHz, $CDCl_3$) δ 7.01 (d, *J* = 15.9 Hz, 1H), 6.59 (ddd, *J* = 10.1, 5.1, 2.2 Hz, 1H), 6.01 (d, *J* = 15.8 Hz, 1H), 5.85 (dd, *J* = 10.2, 2.1 Hz, 1H), 4.77 (d, *J* = 2.5 Hz, 1H), 3.30 (dd, *J* = 3.7, 2.0 Hz, 1H), 3.13 (d, *J* = 1.5 Hz, 1H), 3.03 (d, *J* = 3.9 Hz, 1H), 2.76 – 2.64 (m, 2H), 2.56 – 2.47 (m, 1H), 2.48 (dd, *J* = 2.5, 2.5 Hz, 1H), 2.12 – 2.02 (m, 2H), 1.99 (s, 3H), 1.98 – 1.93 (m, 1H), 1.91 (d, *J* = 1.1 Hz, 3H), 1.88 – 1.60 (m, 4H), 1.48 – 1.41 (m, 2H), 1.40 (s, 3H), 1.36 – 1.24 (m, 3H), 1.17 (s, 3H), 0.88 (s, 3H). **^{13}C NMR** (101 MHz, $CDCl_3$) δ 203.3, 168.7, 141.3, 141.1, 139.7, 129.2, 125.8, 124.7, 78.1, 75.6, 74.9, 73.4, 59.7, 57.5, 56.4, 52.0, 51.9, 51.2, 43.7, 40.4, 36.9, 35.7, 35.2, 28.9, 23.3, 23.3, 21.8, 16.7, 16.1, 14.9, 14.2. **HRMS** (ESI): Exact mass cald for $C_{31}H_{40}NaO_6$ $[M+Na]^+$, 531.3. Found 531.3.

prop-2-yn-1-yl (*S*,2*Z*,4*E*)-6-((4a*R*,4b*S*,6a*S*,7*S*,9a*S*,9b*S*,9c*S*,10a*R*)-4a,6a-dimethyl-4-oxo-4a,4b,5,6,6a,7,8,9,9a,9b,9c,10a-dodecahydro-4*H*-cyclopenta[1,2]phenanthro[9,10-*b*]oxiren-7-yl)-6-hydroxy-2,3-dimethylhepta-2,4-dienoate (**9**): Analytical data for **9**: **TLC** R_f = 0.83 (50% EtOAc/pentanes, CAM stain). $[\alpha]_D^{24°C}$ = –59.6° (c = 0.085, $CHCl_3$). **IR** (film) $\tilde{\nu}$ = 3733, 3597, 3453, 3302, 2926, 2871, 2480, 2361, 2334, 1711, 1662, 1625, 1567, 1454, 1380, 1292, 1214, 1106, 1076, 973, 889, 767, 630 cm^{-1}. **^{1}H NMR** (400 MHz, $CDCl_3$) δ 7.01 (d, *J* = 15.9 Hz, 1H), 6.93 (dd, *J* = 9.7, 6.0 Hz, 1H), 6.42 (d, *J* = 5.9 Hz, 1H), 6.00 (d, *J* = 16.0 Hz, 1H), 5.96 (dd, *J* = 9.7, 0.8 Hz, 1H), 4.77 (d, *J* = 2.5 Hz, 2H), 3.57 (d, *J* = 3.9 Hz, 1H), 3.31 (dd, *J* = 3.8, 1.4 Hz, 1H), 2.49 (dd, *J* = 2.5, 2.5 Hz, 1H), 2.14 – 2.03 (m, 2H), 1.99 (s, 3H), 1.98 – 1.88 (m, 1H), 1.91 (s, 3H), 1.89 – 1.82 (m, 1H), 1.77 – 1.65 (m, 2H), 1.61 (dd, *J* = 11.0, 8.6 Hz, 1H), 1.54 – 1.47 (m, 1H), 1.45 – 1.40 (m, 2H), 1.38 (s, 3H), 1.36 – 1.22 (m, 2H), 1.21 (s, 3H), 0.90 (s, 3H). **^{13}C NMR** (101 MHz, $CDCl_3$) δ 204.4, 168.7, 151.5, 141.3, 141.0, 138.9, 127.1, 125.9, 124.7, 124.2, 78.1, 75.7, 75.0, 59.7, 54.8, 52.4, 52.0, 51.8, 51.0, 43.5, 40.1, 37.4, 35.1, 28.9, 23.5, 23.4, 21.3, 19.6, 16.7, 16.1, 14.0. **HRMS** (ESI): Exact mass cald for $C_{31}H_{38}NaO_5$ $[M+Na]^+$, 513.3. Found 513.3.

4.5. Single crystal X-ray analyses of (*Z*)-7 and 8

Selected crystallographic data of (*Z*)-**7** are summarized as follows: molecular formula $C_{31}H_{43}NO_6$, Mw 525.69, wavelength Cu K_α, (λ = 1.54178 Å), Monoclinic, $P2_1$, *a*: 6.3281(3) Å, *b*: 7.4242(4) Å, *c*: 28.7295(12) Å, α 90°, β 95.892(3)°, γ 90°, V = 1342.61 $Å^3$, D_{cacld} = 1.300 mg/m^{-3}, F(000) = 568, µ = 0.717 mm^{-1}, T = 123 K.

Selected crystallographic data of **8** are summarized as follows: molecular formula $C_{31}H_{40}O_6$, Mw 508.65, wavelength Cu K_α, (λ = 1.54178 Å), Orthorhombic, $P2_12_12_1$, *a*: 6.2944(3) Å, *b*: 11.7168(5) Å, *c*: 35.5369(17) Å, α 90°, β 90°, γ 90°, V = 2620.9(2) $Å^3$, D_{cacld} = 1.289 mg/m^{-3}, F(000) = 1096, µ = 0.708 mm^{-1}, T = 123 K.

Data collection was performed by Dr. Markus Neuburger (University of Basel) on a Bruker Kappa APEX diffractometer. by placing the crystal in the cold stream (123K) of Oxford Cryosystems open-flow nitrogen cryostat with nominal stability of 0.1K.[97] The absorption process applied to the intensities was SADABS.[98] Integration of the frames and data reduction was carried out using APEX2.[99] The structures were solved by direct methods using Superflip.[100] All non-hydrogen atoms were refined anisotropically by full-matrix least-squares on F using CRYSTALS,[101] and computing molecular graphics were done using CAMERON.[102] The data can be obtained free of charge from The Cambridge Crystallographic Data Centre via www.ccdc.cam.ac.uk/data_request/cif.

4.6. Affinity-based protein profiling tests

Human cells A549 were grown in DMEM medium (Sigma Life Sciences) with 2 mM glutamine (PAA) and 10 % fetal bovine serum (Sigma Life Sciences) for analytical (6 well) and for preparative (TC dish 150 standard) studies, respectively. For SILAC studies, SILAC medium (Gibco, Life Technologies) with 2 mM glutamine (PAA), 10% dialysed fetal bovine serum (Sigma Life Sciences) and isotope labelled amino acids (K0, K4, K6, R0, R8, R10; euriso-top) were used. The cells were grown to 70-80 % confluence. Cells were incubated for 1 h with varying concentrations of probe (stock solution in DMSO, 0.1% end concentration of DMSO) in a cell incubator at 37 °C. Subsequently, the cells were scraped off and pelletized for 3 min at 600 g. The pellets were washed with PBS once and then resuspended in lysis buffer (1% (v/v) NP40 and 1% (w/v) sodium deoxycholate) and incubated at 0 °C for 15 min. Membrane and cytosol were separated by centrifugation (20 min, 4 °C, $21 \cdot 10^3$ xG). The membrane fraction was washed once with PBS (1 × 10 sec, 10% maximum intensity) and resuspended in 200 µL PBS for analytical, 1000 µL for preparative analysis.

4.7. *VirtualToxLab* studies

Version 5.8 of *VirtualToxLab* was used for the data presented in this paper. The simulations are conducted at the atomic level and explicitly allow for a mechanistic interpretation of the results. The underlying protocol is independent from any training data and makes the approach universal with respect to the applicability domain. Overall, a toxic potential of a compound is derived from the binding affinities (computed by means of 4D Boltzmann scoring of all binding modes identified through automated, flexible docking to the 3D structure of the target protein) towards a series of 16 proteins known to trigger adverse effects and weighted using the standard deviations of the individual predictions. The individual target proteins screened include: Androgen receptor (AR), Aryl hydrocarbon receptor (AhR), Cytochrome P450 1A2 (CYP1A2), Cytochrome P450 2C9 (CYP2C9), Cytochrome P450 2D6 (CYP2D6), Cytochrome P450 3A4 (CYP3A4), Estrogen receptor α (ERα), Estrogen receptor β (ERβ), Glucocorticoid receptor (GR), hERG, Liver X receptor (LXR), Mineralocorticoid receptor (MR), Peroxisome Proliferator-Activated receptor γ (PPARγ), Progesterone receptor (PR), Thyroid receptor α (TRα), Thyroid receptor β (TRβ). Except for AhR and hERG (for which homology models are employed), all simulations are based on high-resolution crystal structures from the PDB.

4.8. Neurite outgrowth GR competition assay

Human neuroblastoma SH-SY5Y cells (ATCC-CRL-2266) were grown in DMEM/F-12 media (Dulbecco's Modified Eagle Medium F12 Nutrient Mixture HAM, with high glucose and phenol red, without glutamine and HEPES; GIBCO Life Technologies 21331-020) supplemented with 10% fetal bovine serum (FBS South American CE, 10270106 Gibco Life Technologies) and 1% Penicillin-Streptomycin (10,000 U/mL, Life Technologies 15140-122) in canted neck culture flasks with vented cap (75 cm^2, Falcon 353136). Cells were passaged at least three times before use in experiments; for this, 0.25% Trypsin-EDTA solution (Sigma-Aldrich T3924) and Dulbecco's phosphate-buffered saline (DPBS, 1X, without Ca/Mg, pH 7.2, Sigma-Aldrich D8537) were used.

All experiments were performed under strictly sterile conditions. The cells were plated at an optimal concentration of 5×10^5 cells/mL onto Collagen I, coated 24-well plates (Gibco Life Technologies A11428-02) in the presence of the corresponding compounds (1 μM concentration, 0.1% DMSO) to a total well volume of 1 mL, at 37 °C in a humidified atmosphere (5% CO_2 content). For the control experiments, cells were treated with DMSO vehicle (0.1%) as the negative or all-*trans* Retinoic acid (ATRA, Aldrich R2625) as a positive control. The glucocorticoid receptor (GR) control compounds used were dexamethasone (Dex, Sigma-Aldrich D4902) and mifepristone (Mife, RU-486, Sigma-Aldrich M8046).

After a 6-day incubation, the media (1 mL total volume) was aspirated from each of the 24-well plates and washed with PBS (DPBS). The PBS was removed by aspiration, and the cells were fixed with neutral buffered formaldehyde 4% solution (10% formalin, Sigma-Aldrich HT5012; 500 μL) dropped slowly down the side of the well. The plates were incubated at room temperature for 1–2.5 hours and then washed with PBS (1 × 500 μL). The plates were then stained with a thin-layer of Giemsa stain (modified solution, Sigma-Aldrich GS500, 100 μL; previously filtered through a VWR 0.2 μm PES sterile syringe filter and diluted with MeOH) to visualize the cell bodies. After 2 minutes, the stain was diluted with PBS (500 μL) and, after gentle swirling for 2 minutes, the solution was removed by aspiration. The plates were then washed with PBS (1 × 500 μL) and imaged under PBS by phase contrast microscope (160× magnification, Leica DMI 4000B, Germany). When it was necessary, the PBS was aspirated off an additional time and replaced with a fresh layer.

All assays were performed in triplicate, with 6–11 images randomly taken between the three wells, and at least 350 cells counted per treatment per plate (three wells/plate per treatment). Those cells having at least one neurite with a length of more than 50 μm were counted as differentiated (positive). The ratio of neurite positive cells to total cells was evaluated with cell counting tool in ImageJ, and error is represented by the standard error of the mean (SEM). Large cell aggregates were not counted. Plots were drawn using Microsoft Excel. The significance of the results was examined by ANOVA and post hoc tests (Dunnett's Method and Tukey Kramer Method) using Excel. All treatments were significantly different than the DMSO control.

4.9. GR lysate binding bioassay

Recombinant human glucocorticoid receptor α (GR) Baculovirus stock was produced using Bac-to-Bac expression system (Invitrogen). For lysate preparation cells were collected in ice-cold PBS and centrifuged at 3000 g, 4 °C, 10 min, resuspended in binding buffer (pH 7.4, 50 mM HEPES, 10 mM EDTA, 50 mM sodium tungstate, 50% glycerol) and homogenized using a glass puller with 50 strokes. The lysate was centrifuged (16,000 g, 10 min, 4 °C) and supernatants stored at –80 °C.

Recombinant human GR lysate was incubated in the presence of 10 nM [1,2,4,6,7-3H]-Dexamethasone (American Radiolabeled Chemicals, St. Louis, MO) and unlabeled competitor (either 10 μM Dex or 10 μM respectively 1 μM Withanolide A) for 4 h at 16 °C. Free concentration of ligand was separated by adding 5% dextran coated charcoal in binding buffer and incubation on ice for 10 min following centrifugation at 3200 g, 4 °C for 10 min. The GR bound fraction of radioligand in supernatants was measured by scintillation counting.

4.10. GR and MR transactivation bioassay

HEK-293 cells were seeded in poly-L-lysine-coated 24 well plates. Each well contained 80'000 cells cultivated in 500 μL DMEM supplemented with 10% FBS. After 24 h, cells were transfected with 281 ng of TAT3 TATA Luc control plasmid, and 188 ng of plasmid for human GR-α or MR expression using FuGENE (Promega). 24 hours later, cells were washed twice with steroid-free medium, followed by incubation for another 24 h in the presence of steroid hormone (10 nM aldosterone for

MR, 100 nM cortisol for GR), receptor antagonist (1 µM spironolactone for MR and 1 µM Mife for GR) or 1 µM of Withanolide A. Cells were lysed in 60 µL of tropix lysis solution (Applied Biosystems, Foster City, CA) supplemented with 0.5 µM dithiothreitol.

Luciferase activity was determined in 20 µl lysate adding 100 µl of D-luciferin-firefly substrate solution at a final concentration of 0.47 mM D-luciferin, 53 mM ATP, 0.27 mM coenzyme A, 0.13 mM EDTA, 33.3 mM dithiothreitol, 20 mM tricine, pH 7.8, and 8 mM MgSO4. Samples were measured using a SpectraMax-L luminometer (Molecular Devices, Devon, UK). Luciferase activities were used to calculate fold activation compared with vehicle control (0.05% DMSO).

4.11. GR docking studies

Docking was performed using the GOLD 5.2 software (Chambridge Crystallographic Data Centre, Cambridge, UK). This program applies a genetic algorithm for the identification of accurate docking poses for small molecules into the binding pocket of a protein. The crystal structure of GR with the PDB entry 1M2Z was chosen because the initial screenings with the *VirtualToxLab* were based on this structure. First, the co-crystallized ligand Dexamethasone was docked to investigate whether GOLD could restore the original binding orientation and therefore validate the docking settings. The binding site was centered on the carbonyl-oxygen of Asn564 (x 27.23; y 3.52; z 13.23) surrounded by a 9 Å sphere. GoldScore was selected as scoring function. Interactions found for the docking solutions between the ligands and the GR binding pocket were evaluated using LigandScout 3.12. This program automatically analyzes the observed interaction pattern between the docked ligand and the protein, based on the chemical functionalities, the geometric distances and the angles between neighboring structures.[102]

Appendix A. Supplementary Data

Supplementary data can be found online at http://doi.org/xxx/j.bmc.xxx. The probe synthesis, NMR spectra, characterization, target profiling, *VirtualToxLab* and docking studies, and all bioassays are described in this article.

AUTHOR INFORMATION

Corresponding Author

* Tel: +41 44 635 42 81. Email: karl.gademann@uzh.ch.
Homepage: http://www.chem.uzh.ch/research/gademann.html.

Author Contributions

E.C. and K.G. contributed the design of probes, withanolide A isolation, WitA probe synthesis (with E.M.), initial analytical target profiling experiments, GR competition and neurite outgrowth experiments (with L.B.), target profiling data interpretation, and are the main contributors to the manuscript, and primary coordinators of the project. W.H., J.V., and S.S. performed and all target profiling experiments and corresponding data analysis. M.S. and A.V. contributed the *VirtualToxLab* studies and data interpretation. K.R. B., P.S. and A.O. contributed the GR/MR transactivation and binding experiments, and docking studies. E.C., K. G., W. H., S. S., K.R.B., and A. O. wrote the manuscript. All authors approved the manuscript.

Notes

The authors declare no competing financial interest.

ACKNOWLEDGMENT

We thank Dr. Ya-Chu Hsieh for critically proofreading and formatting the manuscript. This research was supported in part by a NIBR Postgraduate Fellowship, and a Marie Curie International Incoming Fellowship within the 7th European Community Framework Programme (FP7/2007-2013) under REA grant agreement N° 623920 (to E.C.). Part of this research was funded through the SNF (200020_163151). A.O., K.R.B. and P.S. were supported by a grant from the Swiss National Science Foundation No 31003A-179400. We thank the Erasmus program, the Nora Baart Foundation (NBS), the Dr. Saal van Zwanenbergstichting Fellowship, and the KNCV Section Organic Chemistry (Wageningen University, Netherlands) for their financial support of E.M. (visiting student from the University of Amsterdam). We also thank the Department of Chemistry at the University of Basel for financial support of L.B. We are grateful to Prof. William Clegg (University of Cambridge, UK) for X-ray crystallographic support, Dr. Heinz Nadig for HRMS analysis (University of Basel), and Dr. Thierry Langer for providing LigandScout software (Inte:Ligand, Vienna, Austria).

ABBREVIATIONS

GR, glucocorticoid receptor, NR3C1; WitA, withanolide A; Dex, Dexamethasone; Mife, mifepristone, RU-486, RU38486; ATRA or RA, all-*trans* retinoic acid; DMSO, dimethyl sulfoxide; BACE1, beta-secretase 1; ADAM10, a disintegrin and metalloproteinase domain-containing protein 10; SAR, structure–activity relationship; QSAR, quantitative structure–activity relationship; SILAC, stable isotope labeling of amino acids in cell culture; MR, mineralocorticoid receptor; Akt, protein kinase B, PKB; ERK1/2, extracellular regulated kinase 1/2; NGF, nerve growth factor; HD, Huntington's disease; AD, Alzheimer's disease; PD, Parkinson's disease; GC, glucocorticoid; ABPP, activity-based protein profiling; NGF, nerve growth factor; Cort, cortisol; Aldo, aldosterone; Spiro, spironolactone; H-bonding, hydrogen bonding.

REFERENCES

(1) Joyner, P. M.; Cichewicz, R. H. Bringing natural products into the fold - exploring the therapeutic lead potential of secondary metabolites for the treatment of protein-misfolding-related neurodegenerative diseases. *Nat Prod Rep.* 2011; 28: 26–47.

(2) EU Commission Public Health. Neurodegenerative Disorders. http://ec.europa.eu/health/major_chronic_diseases/diseases/brain_neurological/index_en.htm (accessed April 5, 2016).

(3) Alzheimer's Association. 2012 Alzheimer's Disease Facts and Figures. http://www.alz.org/downloads/facts_figures_2012.pdf (accessed April 5, 2016).

(4) McGovern Institute. Brain Disorders: By the Numbers. https://mcgovern.mit.edu/brain-disorders/by-the-numbers (accessed April 5, 2016).
(5) Hefti, F. Pharmacology of neurotrophic factors. *Annu Rev Pharmacol Toxicol.* 1997; 37: 239–267.
(6) Kordower, J. H.; Emborg, M. E.; Bloch, J.; Ma, S. Y.; Chu, Y.; Leventhal, L.; McBride, J.; Chen, E. Y.; Palfi, S.; Roitberg, B. Z.; Brown, W. D.; Holden, J. E.; Pyzalski, R.; Taylor, M. D.; Carvey, P.; Ling, Z.; Trono, D.; Hantraye, P.; Deglon, N.; Aebischer, P. Neurodegeneration prevented by lentiviral vector delivery of GDNF in primate models of Parkinson's disease. *Science.* 2000; 290: 767–773.
(7) Aebischer, P.; Ridet, J. Recombinant proteins for neurodegenerative diseases: the delivery issue. *Trends Neurosci.* 2001; 24: 533–540.
(8) Dawbarn, D.; Allen, S. J. Neurotrophins and neurodegeneration. *Neuropathol Appl Neurobiol.* 2003; 29: 211–230.
(9) Tuszynski, M. H.; Thal, L.; Pay, M.; Salmon, D. P.; U, H. S.; Bakay, R.; Patel, P.; Blesch, A.; Vahlsing, H. L.; Ho, G.; Tong, G.; Potkin, S. G.; Fallon, J.; Hansen, L.; Mufson, E. J.; Kordower, J. H.; Gall, C.; Conner, J. A phase 1 clinical trial of nerve growth factor gene therapy for Alzheimer disease. *Nat Med.* 2005; 11: 551–555.
(10) Bulic, B.; Pickhardt, M.; Schmidt, B.; Mandelkow, E. M.; Waldmann, H.; Mandelkow, E. Development of tau aggregation inhibitors for Alzheimer's disease. *Angew Chem Int Ed.* 2009; 48: 1740–1752.
(11) Tohda, C.; Kuboyama, T.; Komatsu, K. Search for natural products related to regeneration of the neuronal network. *Neurosignals.* 2005; 14: 34–45.
(12) Wilson, R. M.; Danishefsky, S. J. Applications of total synthesis to problems in neurodegeneration: Fascinating chemistry along the way. *Acc Chem Res.* 2006; 39: 539–549.
(13) Wilson, R. M.; Danishefsky, S. J. Small molecule natural products in the discovery of therapeutic agents: The synthesis connection. *J Org Chem.* 2006; 71: 8329–8351.
(14) Jessen, H. J.; Barbaras, D.; Hamburger, M.; Gademann, K. Total Synthesis and Neuritotrophic Activity of Farinosone C and Derivatives. *Org Lett.* 2009; 11: 3446–3449.
(15) Bonazzi, S.; Eidam, O.; Guttinger, S.; Wach, J. Y.; Zemp, I.; Kutay, U.; Gademann, K. Anguinomycins and derivatives: total syntheses, modeling, and biological evaluation of the inhibition of nucleocytoplasmic transport. *J Am Chem Soc.* 2010; 132: 1432–1442.
(16) Wach, J. Y.; Gademann, K. Reduce to the Maximum: Truncated Natural Products as Powerful Modulators of Biological Processes. *Synlett.* 2012; 163–170.
(17) Schmid, F.; Jessen, H. J.; Burch, P.; Gademann, K. Truncated militarinone fragments identified by total chemical synthesis induce neurite outgrowth. *Med Chem Commun.* 2013; 4: 135–139.
(18) Crane, E. A.; Gademann, K. Capturing Biological Activity in Natural Product Fragments by Chemical Synthesis. *Angew Chem Int Ed.* 2016; 55: 3882–3902.
(19) Subramanian, S. S.; Sethi, P. D.; Glotter, E.; Kirson, I.; Lavie, D. 5,20(alpha)(R)-Dihydroxy-6(alpha),7(alpha)-Epoxy-1-Oxo-(5(alpha)) Witha-2,24-Dienolide, New Steroidal Lactone from Withania Coagulans. *Phytochemistry.* 1971; 10: 685–688.
(20) Sangwan, R. S.; Chaurasiya, N. D.; Misra, L. N.; Lal, P.; Uniyal, G. C.; Sharma, R.; Sangwan, N. S.; Suri, K. A.; Qazi, G. N.; Tuli, R. Phytochemical variability in commercial herbal products and preparations of Withania somnifera (Ashwagandha). *Curr Sci.* 2004; 86: 461–465.
(21) Kulkarni, S. K.; Dhir, A. Withania somnifera: an Indian ginseng. *Prog. Neuropsychopharmacol Biol Psychiatry.* 2008; 32: 1093–1105.
(22) Chatterjee, S.; Srivastava, S.; Khalid, A.; Singh, N.; Sangwan, R. S.; Sidhu, O. P.; Roy, R.; Khetrapal, C. L.; Tuli, R. Comprehensive metabolic fingerprinting of Withania somnifera leaf and root extracts. *Phytochemistry.* 2010; 71: 1085–1094.
(23) Kuboyama, T.; Tohda, C.; Zhao, J.; Nakamura, N.; Hattori, M.; Komatsu, K. Axon- or dendrite-predominant outgrowth induced by constituents from Ashwagandha. *Neuroreport.* 2002; 13: 1715–1720.
(24) Aggarwal, B. B.; Ichikawa, H.; Garodia, P.; Weerasinghe, P.; Sethi, G.; Bhatt, I. D.; Pandey, M. K.; Shishodia, S.; Nair, M. G. From traditional Ayurvedic medicine to modern medicine: identification of therapeutic targets for suppression of inflammation and cancer. *Expert Opin Ther Targets.* 2006; 10: 87–118.
(25) Jain, S.; Shukla, S. D.; Sharma, K.; Bhatnagar, M. Neuroprotective effects of Withania somnifera Dunn. in hippocampal sub-regions of female albino rat. *Phytother Res.* 2001; 15: 544–548.
(26) Soman, S.; Korah, P. K.; Jayanarayanan, S.; Mathew, J.; Paulose, C. S. Oxidative stress induced NMDA receptor alteration leads to spatial memory deficits in temporal lobe epilepsy: ameliorative effects of Withania somnifera and Withanolide A. *Neurochem Res.* 2012; 37: 1915–1927.
(27) Chen, L. X.; He, H.; Qiu, F. Natural withanolides: an overview. *Nat Prod Rep.* 2011; 28: 705–740.
(28) Zhang, H.; Timmermann, B. N. Withanolide Structural Revisions by C NMR Spectroscopic Analysis Inclusive of the gamma-Gauche Effect. *J Nat Prod.* 2016, 79, 732–742.
(29) Choudhary, M. I.; Yousuf, S.; Nawaz, S. A.; Ahmed, S.; Atta ur, R. Cholinesterase inhibiting withanolides from Withania somnifera. *Chem Pharm Bull.* 2004; 52: 1358–1361.
(30) Riaz, N.; Malik, A.; Aziz ur, R.; Nawaz, S. A.; Muhammad, P.; Choudhary, M. I. Cholinesterase-inhibiting withanolides from Ajuga bracteosa. *Chem Biodiversity.* 2004; 1: 1289–1295.
(31) Machin, R. P.; Veleiro, A. S.; Nicotra, V. E.; Oberti, J. C.; J, M. P. Antiproliferative activity of withanolides against human breast cancer cell lines. *J Nat Prod.* 2010; 73: 966–968.
(32) Zhang, H.; Samadi, A. K.; Cohen, M. S.; Timmermann, B. N. Anti-proliferative withanolides from the Solanaceae: a structure-activity study. *Pure Appl Chem.* 2012; 84: 1353–1367.
(33) Grover, A.; Shandilya, A.; Agrawal, V.; Bisaria, V. S.; Sundar, D. Computational evidence to inhibition of human acetyl cholinesterase by withanolide a for Alzheimer treatment. *J Biomol Struct Dyn.* 2012; 29: 651–662.
(34) Zhao, J.; Nakamura, N.; Hattori, M.; Kuboyama, T.; Tohda, C.; Komatsu, K. Withanolide derivatives from the roots of Withania somnifera and their neurite outgrowth activities. *Chem Pharm Bull.* 2002; 50: 760–765.

(35) Kuboyama, T.; Tohda, C.; Komatsu, K. Neuritic regeneration and synaptic reconstruction induced by withanolide A. *Br J Pharmacol.* 2005; 144: 961–971.
(36) Patil, S. P.; Maki, S.; Khedkar, S. A.; Rigby, A. C.; Chan, C. Withanolide A and asiatic acid modulate multiple targets associated with amyloid-beta precursor protein processing and amyloid-beta protein clearance. *J Nat Prod.* 2010; 73: 1196–1202.
(37) Jana, C. K.; Hoecker, J.; Woods, T. M.; Jessen, H. J.; Neuburger, M.; Gademann, K. Synthesis of withanolide A, biological evaluation of its neuritogenic properties, and studies on secretase inhibition. *Angew Chem Int Ed.* 2011; 50: 8407–8411.
(38) Liffert, R.; Hoecker, J.; Jana, C. K.; Woods, T. M.; Burch, P.; Jessen, H. J.; Neuburger, M.; Gademann, K. Withanolide A: synthesis and structural requirements for neurite outgrowth. *Chem Sci.* 2013; 4: 2851–2857.
(39) (a) Gersch, M.; Kreuzer, J.; Sieber, S. A. Electrophilic natural products and their biological targets. *Nat Prod Rep.* 2012; 29: 659–682, Krysiak, J.; Breinbauer, R. Activity-Based Protein Profiling for Natural Product Target Discovery. *Top Curr Chem.* 2012; 324: 43–84, (b) Bottcher, T.; Sieber, S. A. beta-Lactams and beta-lactones as activity-based probes in chemical biology. *Med Chem Commun.* 2012; 3: 408–417, (c) Pichler, C. M.; Krysiak, J. Breinbauer, R. Target identification of covalently binding drugs by activity-based protein profiling (ABPP). *Bioorg. Med. Chem.* 2016, 24, 3291-3303, and references cited therein.
(40) Selected examples: (a) Yokota, Y.; Bargagna-Mohan, P.; Ravindranath, P.P.; Kim, K.B.; Mohan, R. Development of withaferin A analogs as probes of angiogenesis**.** *Bioorg. Med. Chem. Lett.*, 2006; 16, p. 2603-2607; (b) Bargagna-Mohan, P.; Hamza, A.; Kim, Y.; Khuan, Y.; Ho, A.; Mor-Vaknin, N.; Wendschlag, N.; Liu, J.; Evans, R.M.; Markovitz, D.M.; Zhan, C.; Kim, K.B.; Mohan, R.. The Tumor Inhibitor and Antiangiogenic Agent Withaferin A Targets the Intermediate Filament Protein Vimentin. *Chem. Biol.*, 2007; 14, 623-634; (c) Falsey, R. R., Marron, M. T., Gunaherath, G. M. K. B., Shirahatti, N., Mahadevan, D., Gunatilaka, L., & Whitesell, L., Actin microfilament aggregation induced by withaferin A is mediated by annexin II. *Nat. Chem. Biol.*, 2006; 2, 33-38
(41) Grossman, E. A.; Ward, C. C.; Spradlin, J. N.; Bateman, L. A.; Huffman, T. R.; Miyamoto, D. K.; Kleinman, J. I.; Nomura, D. K. Covalent Ligand Discovery against Druggable Hotspots Targeted by Anti-cancer Natural Products. *Cell Chem. Biol.* 2017; 24: 1368-1376.
(42) Heydenreuter, W.; Kunold, E.; Sieber, S. A. Alkynol natural products target ALDH2 in cancer cells by irreversible binding to the active site. *Chem Commun. (Cambridge, U. K.)* 2015; 51: 15784–15787.
(43) Rostovtsev, V. V.; Green, L. G.; Fokin, V. V.; Sharpless, K. B. A stepwise Huisgen cycloaddition process: Copper(I)-catalyzed regioselective "ligation" of azides and terminal alkynes. *Angew Chem Int Ed.* 2002; 41: 2596–2599.
(44) Tornoe, C. W.; Christensen, C.; Meldal, M. Peptidotriazoles on solid phase: [1,2,3]-triazoles by regiospecific copper(I)-catalyzed 1,3-dipolar cycloadditions of terminal alkynes to azides. *J Org Chem.* 2002; 67: 3057–3064.
(45) Huisgen, R. Centenary Lecture - 1,3-Dipolar Cycloadditions. *P Chem Soc London* 1961; 0: 357–396.
(46) See Supporting Information for X-ray crystallographic data and analysis.
(47) Also see Supporting Information.
(48) Ong, S. E.; Blagoev, B.; Kratchmarova, I.; Kristensen, D. B.; Steen, H.; Pandey, A.; Mann, M. Stable isotope labeling by amino acids in cell culture, SILAC, as a simple and accurate approach to expression proteomics. *Mol Cell Proteomics.* 2002; 1: 376–386.
(49) Eirich, J.; Burkhart, J. L.; Ullrich, A.; Rudolf, G. C.; Vollmar, A.; Zahler, S.; Kazmaier, U.; Sieber, S. A. Pretubulysin derived probes as novel tools for monitoring the microtubule network via activity-based protein profiling and fluorescence microscopy. *Mol BioSyst.* 2012; 8: 2067–2075.
(50) Also see Supporting Information.
(51) For a complete list of the target profiling hits and original data, including data processing, please see Supporting Information.
(52) McEwen, B. S.; De Kloet, E. R.; Rostene, W. Adrenal steroid receptors and actions in the nervous system. *Physiol Rev.* 1986; 66: 1121–1188.
(53) Hayashi, R.; Wada, H.; Ito, K.; Adcock, I. M. Effects of glucocorticoids on gene transcription. *Eur J Pharmacol.* 2004; 500: 51–62.
(54) Buckingham, J. C. Glucocorticoids: exemplars of multi-tasking. *Br J Pharmacol.* 2006; *147 Suppl 1*: S258–268.
(55) Terada, K.; Kojima, Y.; Watanabe, T.; Izumo, N.; Chiba, K.; Karube, Y. Inhibition of Nerve Growth Factor-Induced Neurite Outgrowth from PC12 Cells by Dexamethasone: Signaling Pathways through the Glucocorticoid Receptor and Phosphorylated Akt and ERK1/2. *PLoS One* 2014; 9: e93223.
(56) Mayer, J. L.; Klumpers, L.; Maslam, S.; de Kloet, E. R.; Joels, M.; Lucassen, P. J. Brief treatment with the glucocorticoid receptor antagonist mifepristone normalises the corticosterone-induced reduction of adult hippocampal neurogenesis. *J Neuroendocrinol.* 2006; 18: 629–631.
(57) Oomen, C. A.; Mayer, J. L.; de Kloet, E. R.; Joels, M.; Lucassen, P. J. Brief treatment with the glucocorticoid receptor antagonist mifepristone normalizes the reduction in neurogenesis after chronic stress. *Eur J Neurosci.* 2007; 26: 3395–3401.
(58) Hu, P.; Oomen, C.; van Dam, A. M.; Wester, J.; Zhou, J. N.; Joels, M.; Lucassen, P. J. A single-day treatment with mifepristone is sufficient to normalize chronic glucocorticoid induced suppression of hippocampal cell proliferation. *PLoS One* 2012; 7: e46224.
(59) Behl, C.; Trapp, T.; Skutella, T.; Holsboer, F. Protection against oxidative stress-induced neuronal cell death--a novel role for RU486. *Eur J Neurosci.* 1997; 9: 912–920.
(60) McCullers, D. L.; Sullivan, P. G.; Scheff, S. W.; Herman, J. P. Mifepristone protects CA1 hippocampal neurons following traumatic brain injury in rat. *Neuroscience.* 2002; 109: 219–230.
(61) Ghoumari, A. M.; Dusart, I.; El-Etr, M.; Tronche, F.; Sotelo, C.; Schumacher, M.; Baulieu, E. E. Mifepristone (RU486) protects Purkinje cells from cell death in organotypic

slice cultures of postnatal rat and mouse cerebellum. *Proc Natl Acad Sci U. S. A.* 2003; 100: 7953–7958.
(62) Llorens-Martin, M.; Trejo, J. L. Mifepristone prevents stress-induced apoptosis in newborn neurons and increases AMPA receptor expression in the dentate gyrus of C57/BL6 mice. *PLoS One* 2011; 6: e28376.
(63) Haynes, L. E.; Griffiths, M. R.; Hyde, R. E.; Barber, D. J.; Mitchell, I. J. Dexamethasone induces limited apoptosis and extensive sublethal damage to specific subregions of the striatum and hippocampus: implications for mood disorders. *Neuroscience.* 2001; 104: 57–69.
(64) Vyas, S.; Maatouk, L. Contribution of Glucocorticoids and Glucocorticoid Receptors to the Regulation of Neurodegenerative Processes. *CNS Neurol Disord Drug Targets.* 2013; 12: 1175–1193.
(65) Varadarajan, S.; Breda, C.; Smalley, J. L.; Butterworth, M.; Farrow, S. N.; Giorgini, F.; Cohen, G. M. The transrepression arm of glucocorticoid receptor signaling is protective in mutant huntingtin-mediated neurodegeneration. *Cell Death Differ.* 2015; 22: 1388–1396.
(66) See Supporting Information for full details.
(67) Vedani, A.; Dobler, M.; Smiesko, M. VirtualToxLab - a platform for estimating the toxic potential of drugs, chemicals and natural products. *Toxicol Appl Pharmacol.* 2012; 261: 142–153.
(68) Vedani, A.; Dobler, M.; Hu, Z. Q.; Smiesko, M. OpenVirtualToxLab-A platform for generating and exchanging in silico toxicity data. *Toxicol Lett.* 2015; 232: 519–532.
(69) Access to the VirtualToxLab is available free of charge for academic institutions, public hospitals, governmental agencies, regulatory bodies and non-profit organizations.
(70) All results were obtained with version 5.8 of the VirtualToxLab (March 2016).
(71) See Supporting Information for MD graphics.
(72) Jessen, H. J.; Schumacher, A.; Shaw, T.; Pfaltz, A.; Gademann, K. A unified approach for the stereoselective total synthesis of pyridone alkaloids and their neuritogenic activity. *Angew Chem Int Ed.* 2011; 50: 4222–4226.
(73) Hoecker, J.; Liffert, R.; Burch, P.; Wehlauch, R.; Gademann, K. Caged retinoids as photoinducible activators: implications for cell differentiation and neurite outgrowth. *Org Biomol Chem.* 2013; 11: 3314–3321.
(74) Burch, P.; Binaghi, M.; Scherer, M.; Wentzel, C.; Bossert, D.; Eberhardt, L.; Neuburger, M.; Scheiffele, P.; Gademann, K. Total synthesis of gelsemiol. *Chem Eur J.* 2013; 19,: 2589–2591.
(75) Burch, P.; Chicca, A.; Gertsch, J.; Gademann, K. Functionally Optimized Neuritogenic Farinosone C Analogs: SAR-Study and Investigations on Their Mode of Action. *ACS Med Chem Lett.* 2014; 5: 172–177.
(76) Burch, P.; Schmid, F.; Gademann, K. Neuritogenic surfaces using natural product analogs. *Adv Healthcare Mater.* 2014; 3: 1415–1419.
(77) See Supporting Information for the full statistical analysis.
(78) See Supporting Information for the full statistical analysis, including ANOVA and post hoc test results.
(79) See Supporting Information for the full statistical analysis.
(80) Necela, B. M.; Cidlowski, J. A. Crystallization of the human glucocorticoid receptor ligand binding domain: a step towards selective glucocorticoids. *Trends Pharmacol Sci.* 2003; 24: 58–61.
(81) Schoch, G. A.; D'Arcy, B.; Stihle, M.; Burger, D.; Bar, D.; Benz, J.; Thoma, R.; Ruf, A. Molecular switch in the glucocorticoid receptor: active and passive antagonist conformations. *J Mol Biol.* 2010; 395: 568–577.
(82) Wyttenbach, A.; Arrigo, A. P. *The Role of Heat Shock Proteins during Neurodegeneration in Alzheimer's, Parkinson's and Huntington's Disease* [Online]; In: Madame Curie Bioscience Database. Austin (TX): Landes Bioscience, 2000-2003; Available from: http://www.ncbi.nlm.nih.gov/books/NBK6495/ (accessed April 29, 2014).
(83) Ichikawa, H.; Takada, Y.; Shishodia, S.; Jayaprakasam, B.; Nair, M. G.; Aggarwal, B. B. Withanolides potentiate apoptosis, inhibit invasion, and abolish osteoclastogenesis through suppression of nuclear factor-kappaB (NF-kappaB) activation and NF-kappaB-regulated gene expression. *Mol Cancer Ther.* 2006; 5: 1434–1445.
(84) Pratt, W. B.; Morishima, Y.; Murphy, M.; Harrell, M. Chaperoning of glucocorticoid receptors. *Handb Exp Pharmacol.* 2006; 172: 111–138.
(85) Falsey, R. R.; Marron, M. T.; Gunaherath, G. M.; Shirahatti, N.; Mahadevan, D.; Gunatilaka, A. A.; Whitesell, L. Actin microfilament aggregation induced by withaferin A is mediated by annexin II. *Nat Chem Biol.* 2006; 2: 33–38.
(86) Kaileh, M.; Vanden Berghe, W.; Heyerick, A.; Horion, J.; Piette, J.; Libert, C.; De Keukeleire, D.; Essawi, T.; Haegeman, G. Withaferin A strongly elicits I kappa B kinase beta hyperphosphorylation concomitant with potent inhibition of its kinase activity. *J Biol Chem.* 2007; 282: 4253–4264.
(87) Singh, D.; Aggarwal, A.; Maurya, R.; Naik, S. Withania somnifera inhibits NF-kappaB and AP-1 transcription factors in human peripheral blood and synovial fluid mononuclear cells. *Phytother Res.* 2007; 21: 905–913.
(88) Xu, Y. M.; Marron, M. T.; Seddon, E.; McLaughlin, S. P.; Ray, D. T.; Whitesell, L.; Gunatilaka, A. A. 2,3-Dihydrowithaferin A-3beta-O-sulfate, a new potential prodrug of withaferin A from aeroponically grown Withania somnifera. *Bioorg Med Chem.* 2009; 17: 2210–2214.
(89) Ozorowski, G.; Ryan, C. M.; Whitelegge, J. P.; Luecke, H. Withaferin A binds covalently to the N-terminal domain of annexin A2. *Biol Chem.* 2012; 393: 1151–1163.
(90) Khedgikar, V.; Kushwaha, P.; Gautam, J.; Verma, A.; Changkija, B.; Kumar, A.; Sharma, S.; Nagar, G. K.; Singh, D.; Trivedi, P. K.; Sangwan, N. S.; Mishra, P. R.; Trivedi, R. Withaferin A: a proteasomal inhibitor promotes healing after injury and exerts anabolic effect on osteoporotic bone. *Cell Death Dis.* 2013; 4: e778.
(91) Wijeratne, E. M.; Xu, Y. M.; Scherz-Shouval, R.; Marron, M. T.; Rocha, D. D.; Liu, M. X.; Costa-Lotufo, L. V.; Santagata, S.; Lindquist, S.; Whitesell, L.; Gunatilaka, A. A. Structure-activity relationships for withanolides as inducers of the cellular heat-shock response. *J Med Chem.* 2014; 57: 2851–2863.
(92) Gu, M.; Yu, Y.; Gunaherath, G. M.; Gunatilaka, A. A.; Li, D.; Sun, D. Structure-activity relationship (SAR) of

withanolides to inhibit Hsp90 for its activity in pancreatic cancer cells. *Invest New Drugs.* 2014; 32: 68–74.
(93) The quality and content of withanolide A in the Ashwagandha root may vary. In general, it was found that smaller, high quality packages contain relatively more withanolide A.
(94) Structure confirmed by data from Misra, L.; Mishra, P.; Pandey, A.; Sangwan, R. S.; Sangwan, N. S.; Tuli, R. Withanolides from Withania somnifera roots. *Phytochemistry*. 2008; 69: 1000–1004.
(95) Matches isolation data from: (a) Subramanian, S. S.; Sethi, P. D.; Glotter, E.; Kirson, I.; Lavie, D. 5,20α(R)-dihydroxy-6α,7α-epoxy-1-oxo-(5α)witha-2,24-dienolide, a new steroidal lactone from withania coagulans. *Phytochemistry.* 1971; 10: 685–688.; and data in (b) Liffert, R.; Hoecker, J.; Jana, C. K.; Woods, T. M.; Burch, P.; Jessen, H. J.; Neuburger, M.; Gademann, K. Withanolide A: synthesis and structural requirements for neurite outgrowth. *Chem Sci.* 2013; 4: 2851–2857. and (c) Jana, C. K.; Hoecker, J.; Woods, T. M.; Jessen, H. J.; Neuburger, M.; Gademann, K. Synthesis of Withanolide A, Biological Evaluation of Its Neuritogenic Properties, and Studies on Secretase Inhibition. *Angew Chem Int Ed.* 2011; 50: 8407–8411.
(96) Trofimov, B. A.; Tarasova, O. A.; Sigalov, M. V.; Mikhaleva, A. I. The base-catalysed rearrangement of O-propargyl ketoximes to N-1-alkenyl acryl amides. *Tetrahedron Lett.* 1995; 36: 9181–9184.
(97) Cosier, J.; Glazer, A. M. A Nitrogen-Gas-Stream Cryostat for General X-ray Diffraction Studies. *J Appl Cryst.* **1986**, 105–107.
(98) Siemens Industrial Automation, Inc. (1996). SADABS: Area-Detector Absorption Correction; Madison, WI.
(99) Bruker Analytical X-ray Systems, Inc. Apex2 2006, Version 2 User Manual, M86-E01078, Madison, WI.
(100) Palatinus, L.; Chapuis, G. J. SUPERFLIP – a computer program for the solution of crystal structures by charge flipping in arbitrary dimensions. *J Appl Cryst.* 2007; 40: 786–790.
(101) Betteridge, P. W.; Carruthers, J. R.; Cooper, R. I.; Prout, K.; Watkin, D. J. CRYSTALS version 12: software for guided crystal structure analysis. *J Appl Cryst.* 2003; 36: 1487.
(102) Watkin, D. J.; Prout, C. K.; Pearce, L. J. (1996). CAMERON, Chemical Crystallography Laboratory, Oxford, UK.
(102) Wolber G,; Langer T. T. LigandScout: 3-D Pharmacophores Derived from Protein-Bound Ligands and Their Use as Virtual Screening Filters. *J Chem Inf Comput Sci.* 2005; 45: 160–169.

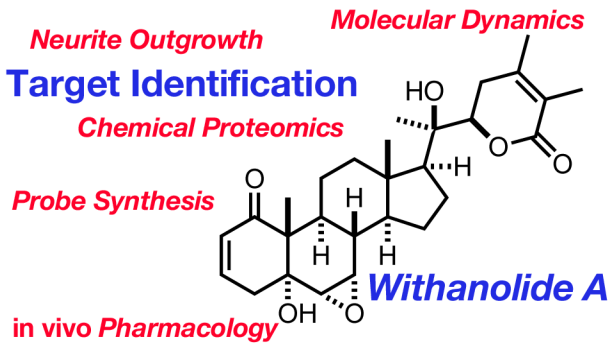
Molecular Dynamics
Neurite Outgrowth
Target Identification
Chemical Proteomics
Probe Synthesis
in vivo Pharmacology
HO
O
O
H
O
H
H
H
OH
O
Withanolide A